Spring 5-2023

HYDROTHERMAL FLUID TRANSPORT PATHWAYS ALONG FRACTURES AND VEINS AT BROTHERS VOLCANO, SOUTHERN KERMADEC ARC

Robert Atnip

HYDROTHERMAL FLUID TRANSPORT PATHWAYS ALONG FRACTURES AND

VEINS AT BROTHERS VOLCANO, SOUTHERN KERMADEC ARC

by

Robert T. Atnip

A Thesis
Submitted to the Graduate School,
the College of Arts and Sciences
and the School of Biological, Environmental, and Earth Sciences
at The University of Southern Mississippi
in Partial Fulfillment of the Requirements
for the Degree of Master of Science

Approved by:

Dr. Jeremy Deans, Committee Chair
Dr. Alyson Brink
Dr. Franklin Heitmuller

May 2023

ABSTRACT

Hydrothermal fluid flow in fractures and veins is a key component in the mineralization of economic metals within calderas. But there are several methods by which fractures can form. Regional extension, episodic caldera collapse, and fluid overpressure all have the potential to create brittle features. Current studies focus on the formation of fractures and veins by these methods, but do not focus on the preferred movement of hydrothermal fluids through brittle features, nor which features are more dominant in active hydrothermal systems. This thesis introduces multiple studies to better understand which method of fracture creation dominates Brothers volcano. Data from IODP Exp. 376 shipboard scientists and post expedition studies were used for paleomagnetic reorientation, downhole linear regression correlation of defining characteristics, and thin section observation. This study finds that regional tectonics are limited in their control over fracture formation, and that fluid overpressure and episodic collapse play a larger role in creating preferred pathways for hydrothermal fluid movement. We expect the results of this study to provide better insight on mineralization of young, developing hydrothermal systems that may be targets for economic drilling.

ACKNOWLEDGMENTS

DEDICATION

To my loving wife, Jac. I could read every publication and book in the history of the world, but there would not be enough words to describe how much your support has meant to me over the years. Thank you for embarking on this adventure with me. You truly are a gem that any geologist would be lucky to find. I love you with all my heart.

To my dogs, Moose and Bucky. The many walks, pets, and distractions were very welcome. You are the best dogs in the world, and deserve all the treats.

To my family, friends, and instructors in Georgia. Thank you for all the support and encouragement over the many years. I am forever grateful for all you have done and continue to do for me.

TABLE OF CONTENTS

LIST OF TABLES

LIST OF ILLUSTRATIONS

CHAPTER I – INTRODUCTION

Brothers volcano (Figure 1.1), a caldera formed in a back-arc due to convergence of the Australian and Pacific plates, hosts the most active hydrothermal system of several volcanic systems along the NE-SW striking Kermadec arc (de Ronde et al., 2001). Brothers volcano hosts two distinct hydrothermal systems: a high temperature, gas-poor fluid that discharges on the NW rim of the caldera, and a lower temperature, gas-rich fluid that discharges on the resurgent Upper Cone (Baker et al., 2012). Volcanogenic massive sulfide (VMS) deposits, which form as sulfur-bearing minerals that precipitate out of hydrothermal fluids, are likely to host economically valuable metals such as gold, silver, copper, zinc, and lead. Given these attributes, Brothers volcano provides a unique opportunity to study an active volcanic system in order to better understand the movement of hydrothermal fluids in a caldera and the role said fluids have on the formation of VMS deposits. Because eruptive material and subsequent mass wasting events usually bury these structurally controlled pathways, they are often only modelled (Gruen et al., 2012; Stix et al., 2003). The International Ocean Discovery Program (IODP) Expedition 376, Brothers Arc Flux, provides one of the first records of sub-seafloor sampling of an actively developing hydrothermal system in an arc setting by coring several holes across five sites, including sites at each type of hydrothermal system (de Ronde et al. 2019). This study will focus on Sites U1527 and U1530 located along the NW caldera wall and Site U1528 located on the resurgent Upper Cone. IODP Exp.

376 sampled fractures and veins that will be used in this study to constrain the fluid

pathways in two distinct, active hydrothermal systems.
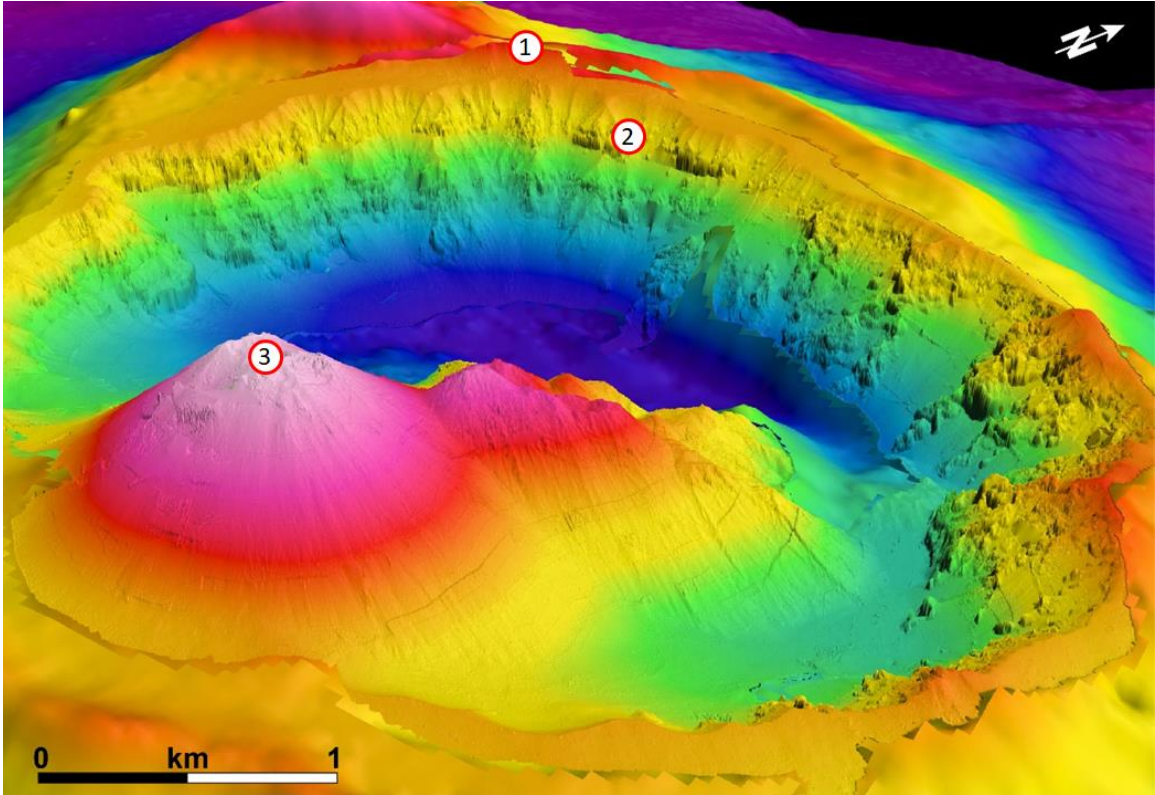
Figure 1.1

3-d bathymetry of Brothers volcano. The general location of the sites for this study are marked as follows: 1 – Site U1527; 2 – Site

U1530; 3 – Site U1528 (from de Ronde et al., 2019).

Hydrothermal fluids develop when water becomes heated and interacts with the crust. Water, sourced from fresh water, seawater, or exsolved from a magma chamber, interacts with the rock and results in fluids of different composition, temperature, and pH. The two hydrothermal systems at Brothers volcano can be identified by the mineralogical components of the vein fill, which relates directly to the fluid input. Identifying the behavior of fractures and veins (e.g., closure, reopening, expansion) can help determine if there were periods of episodic mineralization which could indicate changes in fluid source. Vein mineral assemblage, mineral texture, and cross-cutting relationships may provide insight regarding the pathways of seawater ingress and magmatic fluid ascension in the caldera system.

Permeability, or the ability of fluids to move through a rock, in the caldera can be influenced by lithology, caldera-generated conduits, fluid residence time, and fluid pH values. While caldera collapse itself may generate faults along the rim that increase fluid flow, evidence suggests that permeability is determined by a collection of factors (e.g., fracture density, alteration, lithology) controlling the movement of fluids at Brothers volcano (Tontini et al., 2019). Even still, locations of low temperature fluids next to high temperature fluids suggest that controls can vary with even the slightest lateral change in proximity (Tontini et al., 2019). Therefore, certain fracture generation methods may take precedence over others with regards to pathway creation at Brothers volcano.

Fractures, and therefore veins, can form from several processes. In Brothers volcano, there are likely three main causes of brittle features: regional WNW-ESE extension in the back arc, fluid overpressure, and/or caldera collapse. Each cause may be identified using orientation, mineral fill geometry, and/or cross-cutting

3

relationships. Because the original orientation of the core samples is not maintained, they must be rotated to obtain the correct alignment. This alignment associates individual fractures and veins with their formation events, as discrete populations of fractures and veins may indicate distinct formation processes. To do so, the magnetic declination of several core pieces determined by Exp. 376 shipboard scientists were aligned with the current magnetic declination, which is approximately north, and any features in that core piece were rotated by the same amount. By examining the shipboard data in 10cm intervals, linear regressions of different characteristics between data from the shipboard scientists and the data observed in this study were obtained to determine if any significant correlation between various factors exists. The goal of obtaining linear regression correlations between two or more downhole characteristics is to better constrain how fracture generation methods may be identified.

CHAPTER II – GEOLOGIC HISTORY

2.1 Tonga-Kermadec Trench

The Tonga-Kermadec Trench, a 1000 km subduction zone off the northern coast of New Zealand, is the result of the Australian Plate overriding the Pacific Plate (Figure 2.1) (Wright 1994). It is one of the fastest subducting convergent boundaries on the planet, with rates of 24 cm/yr in the northern part of the trench and 6 cm/yr in the southern portion (Wright et al. 2000). Behind the Kermadec arc lies the Havre Trough, a back-arc basin structure that is typical of oceanic island arcs at convergent plate boundaries. Basin rifting began approximately 5 mya as the Coville Ridge separated from the Kermadec arc in a WNW-ESE direction (Wright 1994). Along the front-arc, seven stratovolcanoes have developed (Clark, Rumble II, Rumble III, Rumble IV, Rumble V, Silent II, and Tangaroa), while 3 calderas are found on the southern end (Brothers, Healy, and Rumble II West) (Wright 1994; Wright and Gamble 1999). These volcanoes and calderas are aligned with the regional strike. At Brothers volcano, the WSW-ENE trend is parallel to the two ridges along the Upper Cone, as well as two regional lineaments that intersect the caldera (Embley et al., 2012).
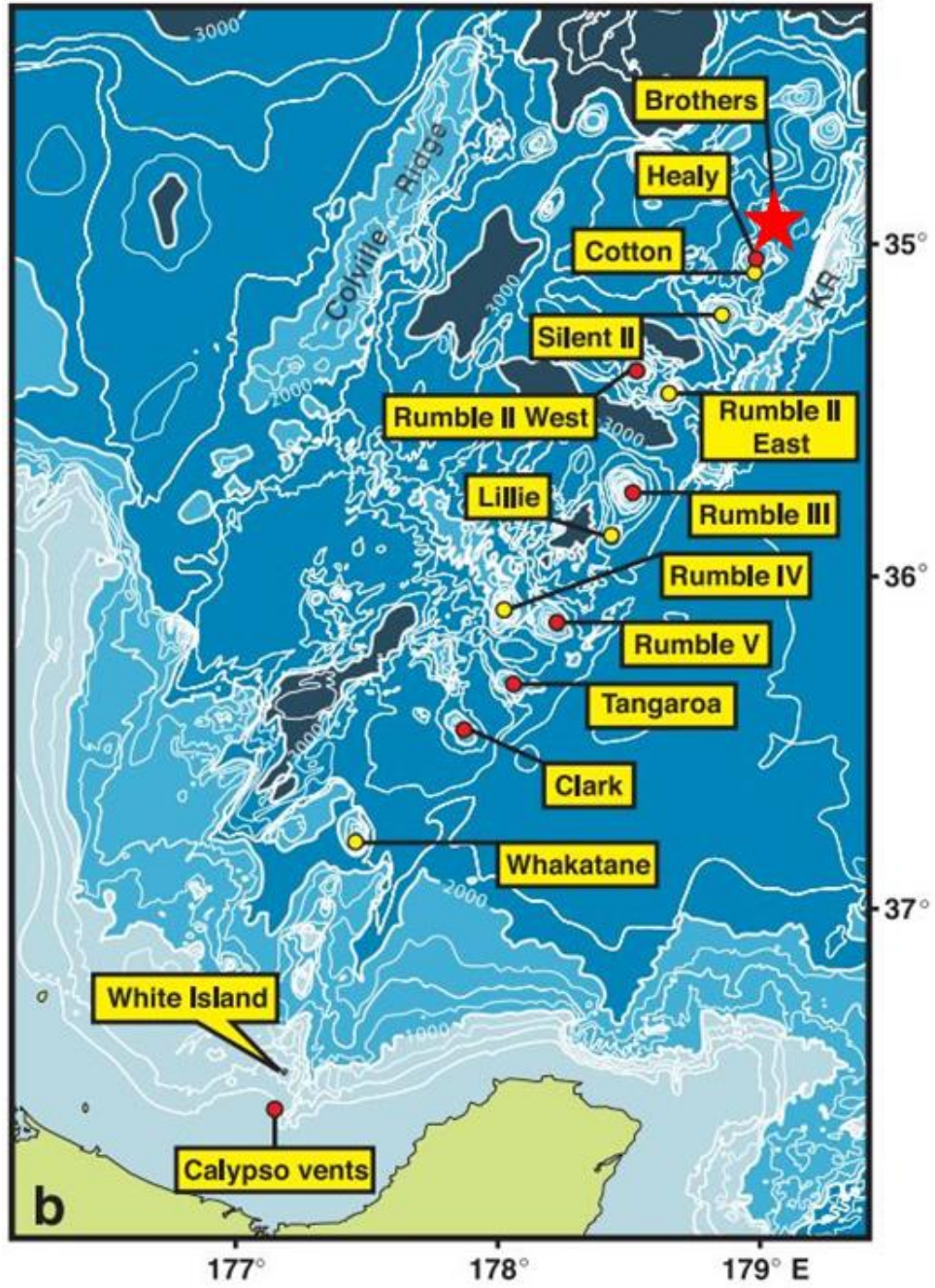
Figure 2.1

Location of Brothers volcano in the northeastern section end of the Kermadec arc. Red dots indicate locations of active venting, while yellow dots indicate either inactive locations or locations with insufficient evidence (from de Ronde et al, 2001).

2.2 Caldera Formation

Calderas develop when a magma chamber below a volcano begins to empty. When a large volume of magma vacates the chamber, the overlying rock collapses into the empty chamber. Caldera collapse often occurs in a piston-like fashion where uniform collapse around the edges of the caldera creates a circular or near-circular shape (Roche et al. 2000). Around the rim of such a symmetrical collapse, a ring of normal faults is arranged around both the wall of the collapse and the piston. In an asymmetrical collapse, however, one part of the caldera falls before the other or more than the other and the collapse is defined by a hinge line on one side of the caldera and a more down-sagged portion on the other, along a normal fault (Figure 2.2) (Walker, 1984; Stix et al., 2003). At Brothers volcano, there is no well-defined ring fault system that would indicate a symmetrical piston-like collapse (Embley et al., 2012). The structure of the caldera is also geometrically asymmetrical, with the longest axis of the ellipse-shaped volcano oriented WNW-ESE (Embley et al., 2012). It is suggested that a hinge line runs parallel to regional extension and through the two resurgent cones in the caldera, implying an asymmetrical collapse that dropped the NW side of the caldera down. This claim can be further supported by greater rim and wall base depths and enhanced hydrothermal activity along the down-sagged NW wall (Embley et al., 2012).
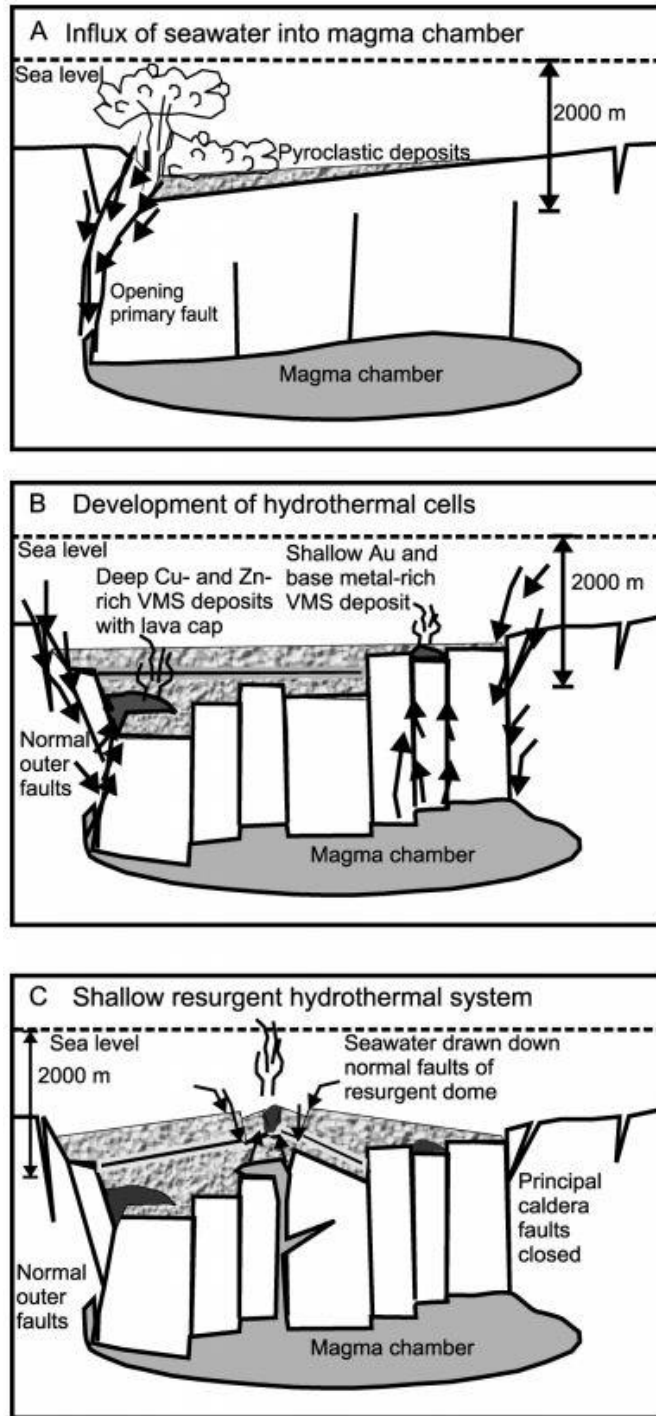
Figure 2.2

The complex process of asymmetrical caldera collapse encourages higher rates of hydrothermal fluid movement and mineral deposition on the down-sagged end (Stix et al. 2003).

2.3 Caldera Faulting and Fracturing

Faulting and fracturing that occurs with caldera collapse creates new conduits for hydrothermal fluids to ascend (Stix et al., 2003). VMS deposits, which are associated with siliciclastic volcanic rocks, have been located globally in arc calderas where magmatically heated sea and/or ground water influxes have interacted with the rock column and moved to the surface (Large et al., 2001). These fault and fracture systems are thought to be the most efficient way for fluids to move through the crust, especially along fault intersections, and is the primary mechanism for models of fluid movement in the crust (Gruen et al., 2012; Stix et al., 2003). Although ring-faulting can account for increased fluid flow, heat studies at Brothers volcano have shown high temperature fluid flow at both the NW caldera wall and the cones, indicating enhanced heating and mass output from a magma chamber (Fig. 2.3) (Tontini et al., 2019). The same study shows locations of cold or low heat flow in close proximity to areas of higher heat flow, which suggests that ring-faulting is not the only factor in fluid permeability in the caldera (Tontini et al., 2019).

2.4 Brothers Volcano

Brothers volcano is a caldera located 1879m below the sea level in the southern portion of the Tonga-Kermadec arc (Embley et al., 2012). The caldera is oval in shape, 3km NNE-SSW and 3.5km WNW-ESE in diameter, with a rim 350-405m above the sea floor (Wright and Gamble 1999). The WNW-ESE regional extensional trend is paralleled by the major axis of the caldera diameter. The caldera walls are sloped 50-60° (Wright and Gamble 1999) and show signs of collapse in the form of possible ring

faulting via near-vertical scarps, terraces, and escarpments (Embley et al., 2012; Wright and Gamble, 1999). The NW caldera wall is comprised of highly altered lava flows covered by volcaniclastic sediment; the degree of alteration suggests a long-term exposure to high-temperature fluid interaction (de Ronde et al., 2011).

Two resurgent cones are located inside the caldera: the Upper Cone and the Lower Cone. The Upper Cone reaches 1196m below sea level; the Lower Cone, by comparison, only reaches 1304m (Embley et al., 2012). The Lower Cone is parasitic of the Upper Cone, shouldering into the NE flank of the latter (de Ronde et al., 2011). Both cones have primarily ash slopes, with large areas of native sulfur that indicate diffuse, low volume venting (de Ronde et al., 2011). The summit of the Upper Cone houses a crater approximately 40m in diameter and 10m deep (de Ronde et al., 2011). Five inactive chimney structures are located on the SE wall of the summit crater of the Upper Cone, indicating previous venting events (de Ronde et al., 2011).

The lithology of the Brothers volcano is basalt to rhyodacite (de Ronde et al. 2019). Lava flows are primarily glassy, porphyritic dacite with phenocrysts of plagioclase and pyroxene (Gamble and Wright, 1995). The low vesicularity of the dacite suggests that it was not part of any pyroclastic eruption, but rather emplaced, possibly through effusive eruptions (de Ronde, 2005). Proximal pyroclastic debris, including lapilli, breccia, ignimbrite, and chimney fragments are placed via eruption or wasting, creating a layered stratigraphy with the dacite lava flows (de Ronde, 2005). Other components and minerals present in petrographic analysis include glass, titanomagnetite, apatite, and zircon (de Ronde, 2005).

A total of five locations were drilled at Brothers volcano by IODP Exp. 376: Sites U1527, U1528, U1529, U1530, and U1531 (de Ronde et al. 2019). The lithology of Site U1527 is comprised of two main units: a dark gray dacite lava with unaltered scoria and pumice lapilli, and hydrothermally altered volcaniclastic breccia, tuff, and lapilli that varies in composition and color (de Ronde et al., 2019a). Site U1528 consists of three units: altered polymict dacitic lapilli tephra, altered volcaniclastic rocks with altered dacite lava subunits, and altered dacite lava flows (de Ronde et al., 2019a). Site U1530 contains five lithologies: clast-supported polymict lapillistone, altered tuffaceous mudstone, siltstone, and sandstone with altered polymict lapillistone, altered plagioclase-phyric lava, altered volcaniclastic rocks, and altered volcanic rock with interlayered altered plagioclase-phyric lava flows (de Ronde et al., 2019a).

2.5 Hydrothermal Fluids

Brothers volcano is host to two distinct hydrothermal systems. The Type 1 system is defined as a high temperature (320° C), gas-poor, moderately acidic fluid, while the Type 2 system is characterized as a lower temperature (<120° C), diffuse, gassy, low pH (as low as 1.9) fluid (Baker et al., 2012; de Ronde et al., 2019). Type 1 fluids are found at the NW and Upper Caldera sites (IODP Sites U1527 and U1530), where the faulting on a greater scale likely enhances hydrothermal fluid flow. Type 1 fluids are rich in chalcopyrite and anhydrite components (Baker et al., 2012; Humphris et al., 1995). Type 2 fluids are found near the Upper and Lower Cones (IODP Sites U1528 and U1531) alongside native sulfur chimneys, and are dominated by sphalerite components (Baker et al., 2012; Humphris et al., 1995). Similar fluid types have also been observed in other

hydrothermal venting locations, such as the TAG active mound along the Mid-Atlantic

Ridge (Humphris et al., 1995) where VMS deposits can also be found.

A convection model best explains the circulation pattern of hydrothermal fluids at

Brothers volcano. These fluids are proposed to move up and down through faults and

fractures at the NW Caldera site, or through permeable breccia that comprises the Upper

and Lower Cones and the caldera floor (Gruen et al., 2012; Tontini et al., 2019). The

convection model can happen on a large scale, where the caldera floor acts as the main

body which seawater percolates through until it is heated by the magma body and ascends

through large faults or fractures on the edges of the caldera (Tontini et al., 2019). These

venting structures are also proximal to cold, down-welling locations, which indicate

zones of shallow recharge (Tontini et al., 2019). Shallow recharge zones permit seawater

to interact with the previously mixed fluids to allow for increased mineralization, as

heavy metals become less soluble with lower temperature (Figure 2.4) (Coumou et al.,

2008; Tontini et al., 2019). These lower temperature fluids represent the diffuse Type 2

fluids documented at the Upper and Lower Cones and in the caldera wall (Baker et al.,

2012).
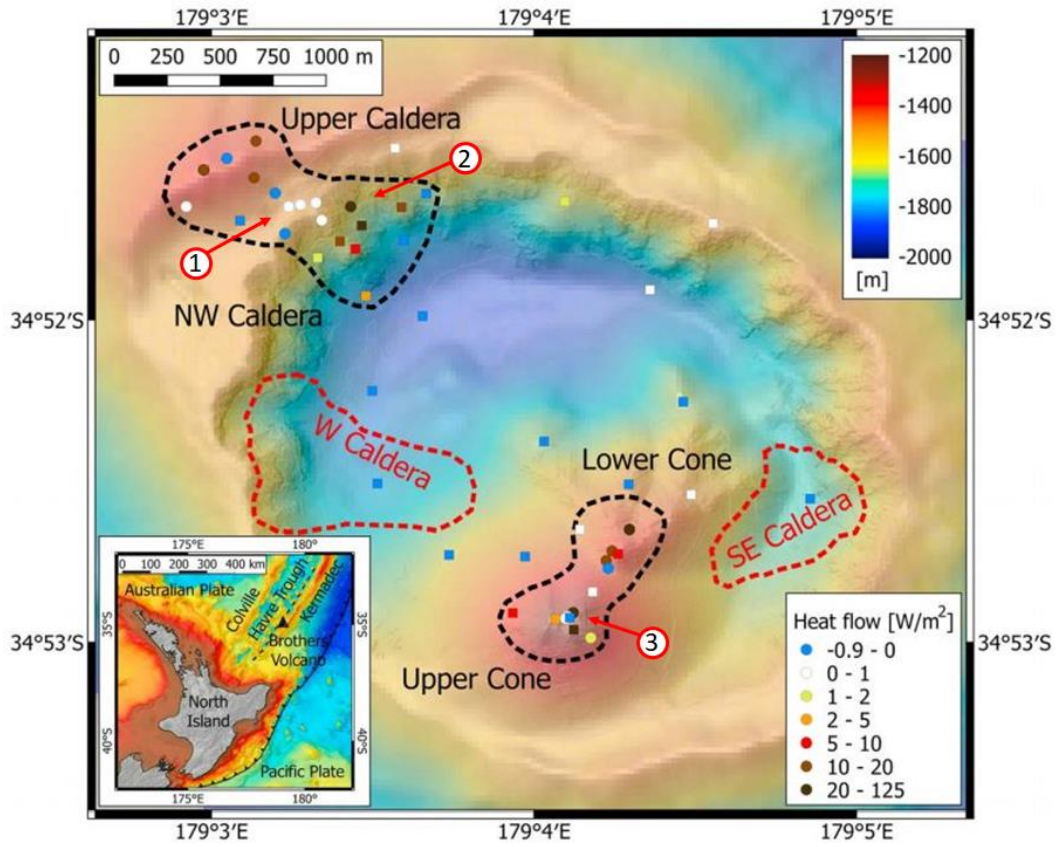
Figure 2.3

Enhanced heat flow map of Brothers volcano with Sites U1527 (1), U1530 (2), and U1528 (3) indicated (from Tontini et al., 2019).
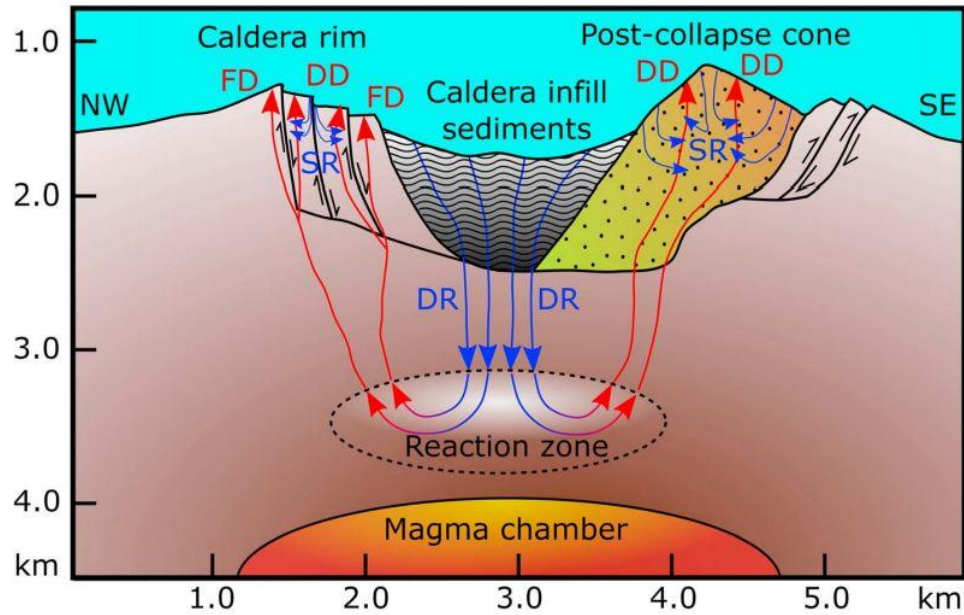
Figure 2.4

Proposed model of hydrothermal fluid circulation at Brothers volcano, with ingress through pyroclastic sediment and ascension along faults/fractures. DD: diffuse discharge; DR: deep recharge; FD: focused discharge: SR: shallow recharge (Tontini et al., 2019).

2.6 Fractures and Veins

Fractures at Brothers volcano can be generated through a few different methods: regional WNW-ESE extension, fluid overpressure, and/or caldera collapse. As fractures develop, they grow in length or branch off from the original fracture and have the potential to intersect with other fractures (Meng et al. 2018). These networks link the pathways for hydrothermal transport and can lead to increased fluid flow and fluid-rock interactions (Figure 2.5). As the vein network grows, dilation of a particular vein (known as the backbone) may occur (Roberts and Sanderson, 1998). This backbone enhances fluid flow by providing a preferred pathway (Roberts and Sanderson, 1998). Discrete veins, which stand apart from a network, act as isolated reservoirs for fluids. However, where discrete veins propagate and intersect networks, a preferred path for fluid movement may be offered.

14

Veins occur when fractures in a rock become filled with solution which then precipitates out a mineral fill. At Brothers volcano, the mineralogical components of veins were recorded at Sites U1527, U1528, and U1530 (de Ronde et al. 2019). Site U1527 is low in vein density; Hole U1527A in particular contains no veins (de Ronde et al. 2019). Hole U1527C contains two veins of quartz and pyrite, both under 1mm thick with a dip of 60° (de Ronde et al. 2019). Site U1530 houses only one hole, Hole U1530A. Hole U1530A contains a large number of veins, filled with anhydrite, pyrite, silica, and clay to a lesser extent (de Ronde et al. 2019). Hole U1530A veins have a large range in dip magnitude (de Ronde et al. 2019). Site U1528 contains an abundance of veins. Hole U1528A contains veins of anhydrite and gypsum, with fewer native sulfur and pyrite veins (de Ronde et al. 2019). Veins in Hole U1528A have a wide range of dip magnitude (de Ronde et al. 2019). Hole U1528C contains only two veins, both filled with clay and native sulfur, with dip magnitudes of 28° and 85° (de Ronde et al. 2019). Hole U1528D contains veins of anhydrite, clay, gypsum, native sulfur, and pyrite (de Ronde et al. 2019). The majority of veins in Hole U1528D have a dip magnitude greater than 45° (de Ronde et al. 2019).

Vein fibers can have preferred orientations. Crystals fibers form when the rate of mineral growth is consistent with its neighboring crystals (Passchier and Trouw, 2005; Ramsay, 1980). If this growth rate is sustained, then the fibers will grow in an orientation in the direction of extension, with vein fiber orientation changing with changes in extension direction. Changes in orientation can be subtle, which may indicate a progressive change in extension direction, or changes in orientation can be abrupt, which may indicate two, discrete opening events (Bons et al. 2012; Passchier and Trouw

2005; Ramsay 1980). Fibers that are randomly oriented would be indicative of events that do not have a sustained stress field over the time period of fiber growth, such as caldera collapse events or fluid over-pressure (Meng et al. 2019). There are two different types of vein growth to consider with respect to vein formation. Syntaxial vein crystals grow from wall to vein center, where as antitaxial vein crystals grow from the center of the vein towards the walls (Passchier and Trouw, 2005). Given that the wall rock is mostly dacite and that most vein minerals (e.g., quartz, pyrite, gypsum, etc.) will not have a duplicate mineral to nucleate on, it is anticipated that most veins will be antitaxial at Brothers volcano. If the vein has not been reopened, then there would be only one expected median line from which growth occurred. If the vein has reopened, which may be expected in this dynamic system, then a crack seal mechanism would best explain the second or later stages of growth (Ramsay, 1980). This reopening would be expected to show growth from a previous plane of fill-wall contact, with inclusions of the wall close to the new plane of growth (Ramsay, 1980).

Veins can also be analyzed for shear sense; a change in rock wall motion would be indicated by curvature of the veins since it is assumed the vein tip will stay parallel to the greatest compressive stress (Passchier and Trouw, 2005). Shear sense can also be determined by shear veins where a change in direction of the vein can lead to a zone of opening (transtension). Furthermore, shear sense can be determined along shear veins by use of steps formed as part of slickensides.

Once a fracture has been filled with mineral precipitate, reopening of the vein causes breakages in the mineral fibers. For the anticipated antitaxial veins at Brothers volcano, that breakage would occur where the mineral fibers meet the wall rock, the

16

weakest plane. There may also be secondary fill in the same vein upon further reopening. If the second source of hydrothermal fluids is the same as the original fracture-filling fluids, then second stage vein fill would be comprised of the same minerals. When the source of the precipitating fluids changes, the second stage vein fill would be expected to change as well. This secondary mineral fill indicates that a different fluid type occupied the vein.
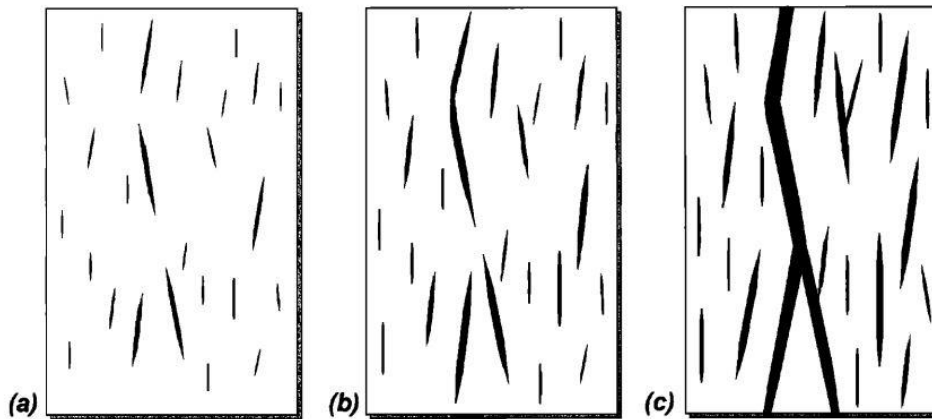
Figure 2.5

Formation of "backbone" veins or preferred pathways (from Roberts and Sanderson, 1998).

CHAPTER III - METHODS

The data used in this study came from several sources. Previous studies that

provided information include DESClogic data collected by IODP Exp. 376 shipboard

scientists, and reorientation data from the research laboratory of Dr. Tontini. Data

generated from this study include reoriented fracture and vein datasets, stereonet plots,

down-core linear regression correlations, and petrographic thin section observations.

Paleomagnetic core realignment of fractures and veins to their true geographic orientation

and construction of stereonets (using Stereonet 11) were completed to visually display

dip and dip-direction for identification of any potential patterns related to fracture/vein

clustering and regional structures. For downcore linear regression correlations, several

different values were used to identify correlations on a heat-map plot using Microsoft

Excel. Thin section analysis allowed for observations of mineral fill and mineral fiber

growth patterns to look for evidence of occupying fluids, reopening events, and potential

influences on fracture/vein origination. Energy dispersive electron microscopy was used

to verify mineral identifications.

3.1 Paleomagnetic Core Realignment

For this study, the paleomagnetic information has been obtained from the

shipboard scientists on IODP Exp. 376 and further expanded upon during laboratory

work from Dr. Fabio Catatori Tontini, Universita di Genova, Italy (de Ronde et al., 2019;

de Ronde et al 2019c). When core pieces are drilled by the IODP vessel *JOIDES*

Resolution (Joint Oceanographic Institutions for Deep Earth Sampling), the core pieces

freely rotate on an axis parallel to the hole in the core barrel and lose their geographic

orientation. As a result, planar features such as fractures and veins do not provide strike

and dip in the geographic reference frame. Instead, planar features are measured based

on a core reference frame determined piece by piece (Fig. 3.1). This results in the

inability to compare structures from piece to piece, hole to hole, or to regional structures.

Each core sample needs to be rotated to its true geographic orientation, and therefore

each fracture and vein may be compared between pieces, holes, the back-arc rift, and the

subduction zone. There are several methods to reorient core; in this study paleomagnetic

realignment is used. This method assumes that the paleomagnetic declination during

eruption is the same as today (due north). The age of the volcano is not known; however,

the average inclination for all sites is indistinguishable from the current geocentric axial

dipole (GAD; inclination of -55°), which indicates a very young age is likely from the

current normal polarity chron. C1n (Cande and Kent, 1995; de Ronde et. al, 2019). It is

important to point out that the paleomagnetic remanent vector (PMRV) inclination is not

affected by core rotation in a vertical hole. By measuring the magnetic field recorded by

magnetic minerals, the paleomagnetic declination in the core reference frame can be

determined for each core piece more than ~5 cm long. The current GAD is due north.

The difference in angle between what is measured in the core reference frame and today's

GAD is the rotation angle used to put core pieces back into the predrilled orientation

relative to geographic north. The rotation angle was added to the azimuthal direction of

veins and fractures to ascertain the true dip direction. One challenge is that some pieces

may not meet length or size requirements to measure magnetic declination (de Ronde et

al., 2019c). Also the GAD can fluctuate/drift with time, so it is not likely to be perfectly

due north. Another issue is that, even if a piece can be realigned, it may not contain

fractures or veins to make it relevant to the study. All of these complications are further

exacerbated by the low recovery during the drilling of Brothers volcano (de Ronde et al.,

2019a).

Stereonets with the true alignment of fractures and veins from Brothers volcano

were plotted with Stereonet 11 software using shipboard structural measurements from

IODP Exp. 376 and post-expedition reorientation data provided from the laboratory of

Dr. Tontini. Stereonets were plotted using Stereonet 11 software and were compared

across all three sites on the volcano as well as each site individually (Allmendinger et al.,

2012; Cardozo and Allmendinger 2013). The paleomagnetic data were compared to

visual core description (VCD) and DESClogic Excel sheets from IODP Exp. 376 to find

core pieces from both datasets that contained discrete fractures/veins with measurable

magnitude dip and dip direction. Once a fracture or vein was identified in a piece that

also had the PMRV measured, the rotation angle was added to the fracture or vein dip

direction in the core reference frame, aligning the fracture or vein to the original, pre-

drilled orientation.
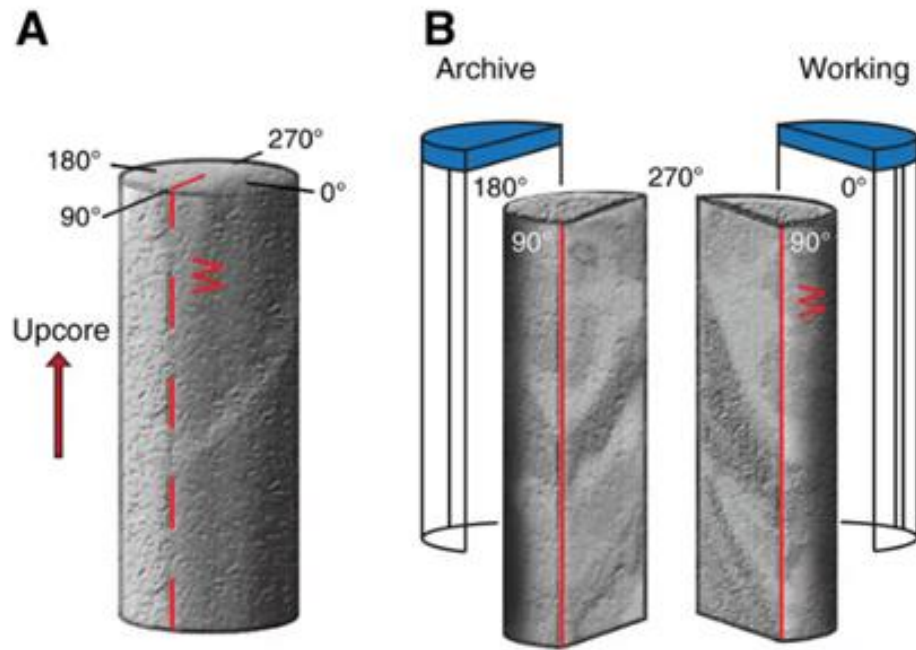
Figure 3.1

Core reference frame as defined by the IODP. "A" illustrates the up-core positioning of the core with reference frame cardinal

directions. "B" displays the core split into the working half ("W") on the right of the cut line; the archived half, on the left, is sent to

one of three IODP core repositories (from de Ronde et al., 2019).

3.2 Downcore Linear Regression Correlations

Core was analyzed by the shipboard party (ref) to obtain depth bin values for

fracture density, vein density, lithology type, alteration intensity, discrete vein total, and

discrete fracture total. This study assigned a numerical value for each lithology type

based on the lithology identified by the shipboard party (de Ronde et al., 2019c) (Table

3.1). Fracture density, vein density, and alteration intensity values are ordinal (de Ronde

et al., 2019) and are used directly from the shipboard data. Fracture density is defined as

the number of open fractures every 10 cm on a scale of 0-3, with 0 being no fractures per

10 cm and 3 being >5 fractures per 10 cm (Fig. 3.2). Vein density uses the same model,

counting every vein in 10 cm but on a scale of 0-5, with 5 being >20 veins per 10 cm. The vein density scale is greater than the fracture density scale to account due to the fact that vein density can be greater in the presence of network veins. Alteration intensity is defined in the IODP Exp. 376 ship report methods on a scale of 0-5, with 0 being unaltered and 5 being completely altered (de Ronde et al., 2019c). Alteration intensity was chosen instead of alteration type, given that alteration intensity better represents fluid-rock interaction for correlation with other variables and is consistently applied across all sites. Discrete vein total includes all veins with a measurable strike and dip; this contrasts with the vein density total, which accounts for both discrete and network veins. Similarly, discrete fracture total includes all fractures with a measurable strike and dip. Discrete fracture and vein totals are collected by counting each one, respectively, in every 10 cm section of core. A Python script was created to complete the depth bin counting process for discrete veins (Appendix A). The script requires a text file input with columns for depth bins and discrete vein depths. The user then gives the desired output file path location. A list is created for both bins and veins. For every bin depth, the veins are iterated and analyzed for depths. If the vein is included in any depth bin, the depth bin total is appended by one. Some discrete veins cross multiple depth bins, and are therefore recorded several times, but only once for each bin. For example, if a discrete vein was recorded at 49-62cm, the 40-49, 50-59, and 60-69 cm bins would each have one added to their totals. There were no horizontal veins, so the code does not include bin counting for discrete horizontal veins; the code can be amended if discrete horizontal veins were to be included. The completed lists were output as text files, with the data copied to Microsoft Excel for correlation plot construction.

To compare multiple variables against each other, a linear regression model was implemented and then plotted using a correlation heatmap. Because multiple variable types and scales were used, variables were normalized on a scale of 0-1 (see below) so data could be analyzed.

$$X_{NORM} = (X\text{-}X_{MAX})/(X_{MAX}\text{-}X_{MIN}) \tag{1}$$

X_{NORM} = normalized variable value

X = variable of interest

X_{MAX} = maximum variable recorded

X_{MIN} = minimum variable recorded

Using the normalized values, a z-score was obtained to reflect changes in standard deviation for each recorded instance of a variable and to further normalize each dataset. The z-score was calculated using the following formula:

$$z = (x\text{-}\mu) / \sigma \tag{2}$$

z = z-score value

x = observed normalized value

μ = mean of the normalized value

σ = standard deviation of the normalized sample

A correlation heatmap was constructed in Excel using the following z-score variables: vein density (VDZ), fracture density (FDZ), lithology type (LithZ), alteration intensity (AltZ), discrete vein total (DVTZ), and discrete fracture total (DFTZ). For correlation results, the following scale is used to indicate strength of relationships:

|0-0.19|: very weak

|0.2-0.39|: weak

23

|0.4-0.59|: moderate

|0.6-0.79|: strong

|0.8-1|: very strong

On heatmaps, positive values are indicated by red shading; negative values are shaded blue. Values on the correlation heatmap range from -1 (negative correlation) to 1 (positive correlation). A value close to 0 indicates there is no discernable correlation between the variables in question. Values that are negative but closer to zero may appear gray/white-to-blue, while values that are positive but close to zero may appear pink/white-to-red.

For Sites U1527 and U1528, data collected from multiple holes were combined to make a composite representation of the holes. For Site U1527, Hole U1527A contained no data below 63 mbsf, and Hole U1527C contained no data above 63 mbsf so the two data sets were combined to create a composite dataset. Due to the geographic proximity of Sites U1527 and U1530, they are described sequentially in the results of the study.

Feature	0	1	2	3	4	5
Open fracture density	No open fractures	<1 per 10 cm	1-5 per 10 cm	>5 per 10 cm		
Vein density	No veins	<1 per 10 cm	1-5 per 10 cm	5-10 per 10 cm	10-20 per 10 cm	>20 per 10 cm

Figure 3.2

Intensity ranks of various features associated with rocks at Brothers volcano (from de Ronde et al., 2019).

Table 3.1

IODP defined lithologies at Brothers Volcano

Lithology	Assigned Numerical Value
Dacite	1
Volcanic	2
Tuff	3
Lapilli-tuff	4
Lapillistone	5
Tuff-breccia	6
Volcaniclastic	7
Clay	8
Siltstone	9
Mudstone	10
Sandstone	11

3.3 Thin Section Analysis

Twenty-six thin sections were examined for fracture and vein analysis, including

six from Site U1527, nine from Site U1530, and 11 from Site U1528. Veins were

assessed to identify the following: (a) primary mineral fill, (b) secondary mineral fill (if

present), (c) presence of cross-cutting veins, (d) systematic, syntaxial, and/or antitaxial

direction of mineral fiber growth, and (e) indicators of movement within vein walls.

Secondly, crystal orientation in the veins was observed to determine the direction of

growth as systematic, syntaxial and/or antitaxial, and to document any record of shearing

or motion of the vein walls.

Using a Nikon Eclipse E600POL microscope, Nikon DS-Fi3 camera, and Nikon

NIS Elements Advanced Research software, thin sections were examined in both plain

polarized light (PPL) and cross-polarized light (XPL). Veins were catalogued by sample

depth in meters below seafloor (mbsf) and assigned labels for recording purposes (Tables

4.12-4.15, Results section). For example, V27-1 represents the first vein in Hole

U1527C. The dominant mineral fill was interpreted as the mineral most visible in the

sample. In instances where two minerals appeared to be equally dominant, both were

recorded as the dominant fills. Accompanying fill minerals were interpreted as minerals

that appeared in visibly smaller quantities than the dominant fill. The thickness (mm) of

each vein was recorded by using a millimeter ruler to scale the measuring device built

into the microscope viewing window. The measured thickness of each vein was adjusted

based on the magnification of the microscope to reflect the true vein thickness. All veins

lacked a uniform thickness; the thin section observation tables in Appendix B reflect the

minimum and maximum observed thickness of all veins in this study.

Veins may contain minerals that are not easily identified using visual inspection.

For these minerals, scanning electron microscopy–energy dispersive electron microscopy

(SEM–EDS) analysis was used. Dr. Michael Blanton from the University of Southern

Mississippi School of Polymer Science and Engineering assisted with EDS analysis,

using a Zeiss SIGMA variable pressure field emission scanning electron microscope (VP-

FESEM) equipped with a Zeiss NTS backscatter electron detector (BSD). The software

used was Zeiss FEG-SEM, SmartSEM, and Noran System 7. The working distance

ranged from 7.1-8.0 mm, with a range of magnification from 50-250x. The voltage for

all samples was 20.00 kV. EDS identifies the elemental components of a mineral by

streaming an electron beam at the mineral and measuring the secondary x-rays it emits.

The resulting spectral analysis graphs the percentage of the elements comprising the

mineral, which are then interpreted by the user. In this study, for example, an unknown

mineral was identified by the EDS analysis indicating a 2:1 ratio of oxide and silica. This

mineral, reported here as unknown silicon dioxide mineral (USDM), has the chemical composition of quartz but did not display the typical undulatory extinction when observed in cross-polarized light (XPL). By using EDS, this study was able to confirm mineral identification performed via visual inspection, as well as identify USDM, native sulfur, and unknown clay minerals (UCM1 and UCM2).

CHAPTER IV – RESULTS

4.1 Paleomagnetic Core Realignment

The results here are only for the fractures and veins that were able to be realigned to the pre-drilled orientation. This is a small population compared to all of the fractures and veins measured by shipboard scientists. Fractures and veins measured in the core reference frame can be evaluated and compared based on dip magnitude; therefore, the results described here focus on dip direction and full orientation (dip/dip direction). Tables are included at the end of each Site subsection for each of the entire fracture and vein datasets, whether reoriented or not.

4.1.1 Volcano-wide Results

Plotted data of reoriented fractures and veins (n=176) from all sites (Figure 4.1) appears to have highly variable dip magnitude and orientation with no easily distinguishable pattern. As such, a reliable stereonet contour could not be produced. There is a noticeable lack of dip magnitude in the 20-40° range, except in the southern direction. On the plot of poles, there are two areas circled. The red circle indicates a grouping of brittle features with a dip magnitude of 10° or less. These sub-horizontal features are not seen at every site. The blue circles signify brittle features that dip either NW (direction of regional extension) or SE (the conjugate direction). The SE dipping features appear on plots from Sites U1527 and U1530 (Fig. 4.2, Fig. 4.3). The NW dipping features can be better seen on plots from Sites U1530 and U1528 (Fig. 4.3, Fig. 4.4). Other groupings that appear on the volcano-wide plot may be more significant when described in the context of two sites (i.e., Site 1527 compared to Site 1530). There are notably more dip magnitudes than at Site U1527 that are <30°, although only 3 fall

28

into a sub-horizontal range of <10º (Figure 4.2). Data from Site U1528 shows a wider range of both dip magnitude values and dip direction than sites U1527 and U5130.

Figure 4.1
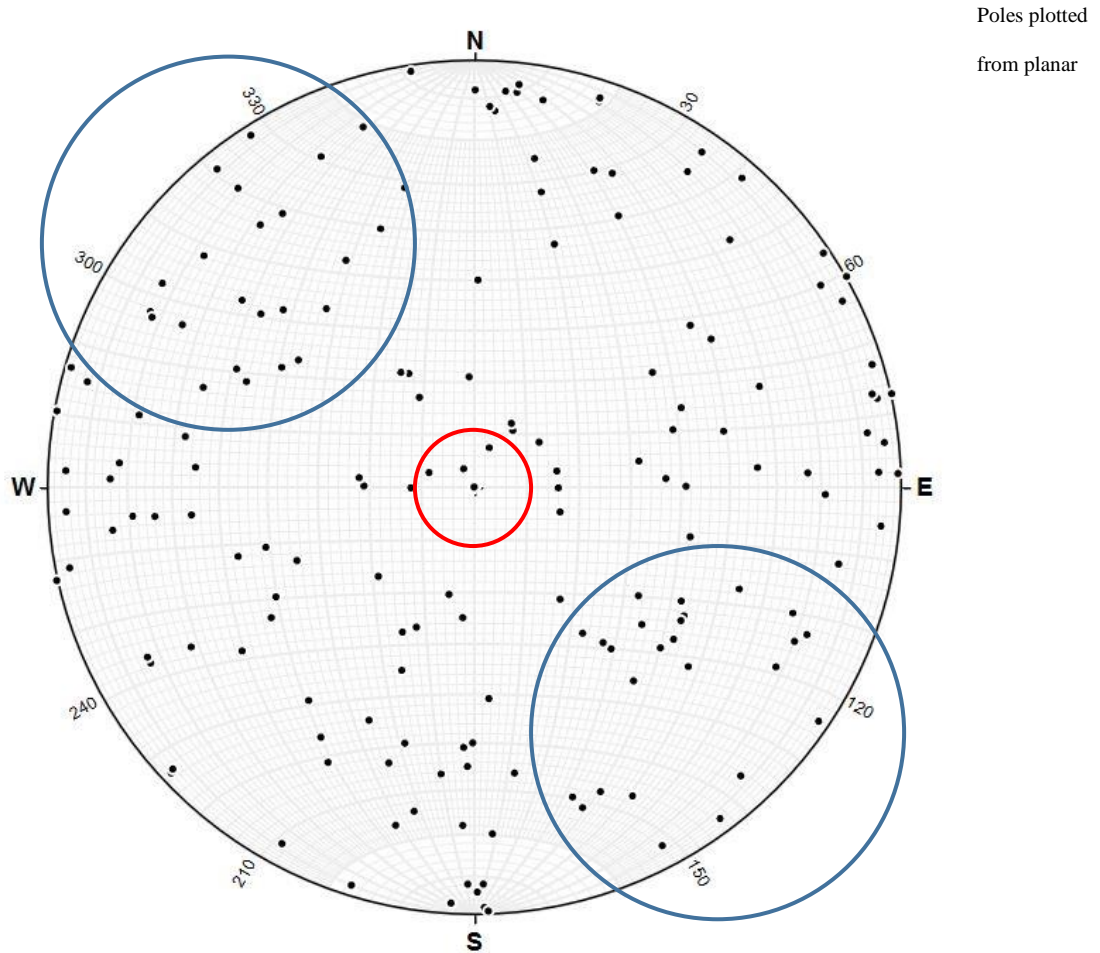
Poles plotted from planar measurements of volcano-wide data from Sites U1527, U1528, and U1530. Two areas of interest shown in colored circles. Red: brittle features with a dip magnitude of 10º or less; blue: brittle features with a dip direction of NW or SE. Circles drawn arbitrarily to signify general areas for observation.

4.1.2 Site U1527

Site U1527 contains the fewest total brittle features (n=31) of all three Sites. The fractures and veins have a wide variation in orientation but do have a generalized NNW or SE dip direction with moderate-to-steep dip values (Figure 4.2). Throughout the site, 10 reoriented fractures occur in several lithologies and alteration types (Table 4.1). The majority of these fractures occur between 200-250 mbsf. There are fewer planar features that fall outside of this grouping, and notably none that would fall into a sub-horizontal category. The total fractures and veins at Site U1527 and their distribution among different lithologies and alteration types are listed below (Table 4.2).
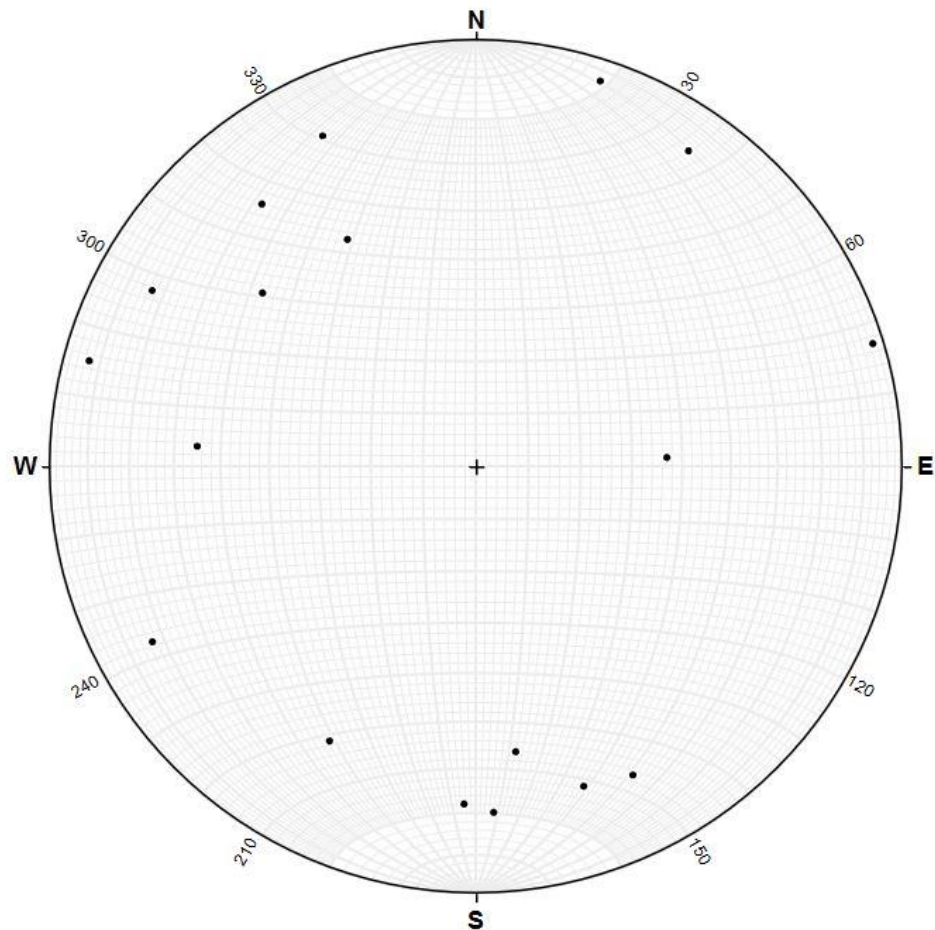
Figure 4.2

Poles to planes of discrete fractures at Site U1527.

Table 4.1

Reoriented fractures located at Site U1527

Fracture/Vein ID	Depth (mbsf)	Azimuthal Orientation	Dip Magnitude	Igneous Unit	Alteration Type
1527-C1-F1	49.3	118.47	75	1	Ia
1527-C1-F2	49.52	150.51	51	1	Ia
1527-C1-F3	186.55	351.98	57	2b	Ib
1527-C1-F4	187.9	155.14	74	2b	Ib
1527-C1-F5	220.27	356.98	70	2b	IIa and IIb
1527-C1-F6	220.35	332.98	70	2b	IIa and IIb
1527-C1-F7	225.91	129.07	54	2c	III
1527-C1-F8	228.67	140.77	68	2c	III
1527-C1-F9	229.69	001.93	68	2d	III
1527-C1-F10	229.76	341.3	68	2d	III

Table 4.2

Distribution of fractures and veins at Site U1527 grouped by lithology and alteration type.

Lithology	Alteration Type	Fracture Total	% Fractures in Site	Vein Total	% Veins in Site	% Planar Features in Site
1	Ia	5	17.24	0	0.00	16.13
2b	IIa	6	20.69	1	50.00	22.58
2b	IIa and IIb	6	20.69	0	0.00	19.35
2c	III	5	17.24	0	0.00	16.13
2d	IIa	7	24.14	1	50.00	25.81

4.1.3 Site U1530

Site U1530 has fractures (17) and veins (64) (n=81) with a majority of moderate dip magnitudes (40-60º). Two clusters of moderate-to-steeply WNW or ESE dipping fractures and veins (6 and 8 total, respectively) can be observed (Fig. 4.3). Fractures in the WNW and ESE clusters are largely confined to a depth range of 160-200 mbsf, while veins in the same cluster occur mostly between 200-400 mbsf (Table 4.3). There is a cluster of 6 moderate-to-steeply SSW dipping veins. These veins are seen throughout the site and do not appear to be confined to any particular depth interval (Table 4.4). The total fractures and veins at Site U1530 and their distribution among different lithologies and alteration types are listed below (Table 4.5).

32
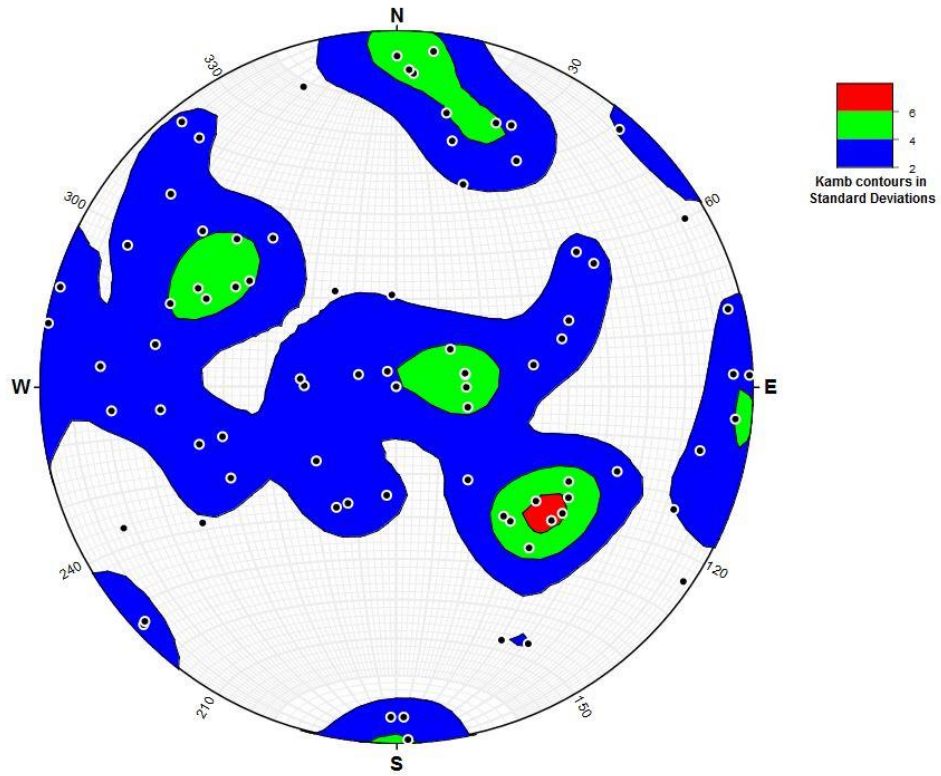
Figure 4.3

Poles to planes of fractures and veins from Site U1530.

Table 4.3

Reoriented fractures located in the WNW or ESE dipping clusters at Site U1530.

Fracture/Vein ID	Depth (mbsf)	Azimuthal Orientation (degrees)	Dip Magnitude (degrees)	Igneous Unit	Alteration Type
1530-C1-V1	51.7	110.2	57	2b	II
1530-C1-F1	165.31	298.83	46	4	IIIb
1530-C1-F2	190.89	302.84	48	4	IV
1530-C1-F3	191.02	121.84	44	4	IV
1530-C1-F4	191.11	114.84	49	4	IV
1530-C1-F5	191.16	125.84	42	4	IV
1530-C1-V2	242.46	309.35	42	5	V
1530-C1-V3	256.47	116.42	52	5	V
1530-C1-V4	271.41	319.74	41	5	II
1530-C1-V5	272.02	310.79	48	5	II
1530-C1-V6	290.35	270.52	16	5	II
1530-C1-V7	314.12	307.34	49	5	V
1530-C1-V8	391.4	132.86	51	5	II
1530-C1-F6	415.22	320.36	39	5	IV

Table 4.4

Reoriented fractures located in the NNE or SSW dipping clusters at Site U1530.

Fracture/Vein ID	Depth (mbsf)	Azimuthal Orientation (degrees)	Dip Magnitude (degrees)	Igneous Unit	Alteration Type
1530-C1-V1	22.24	183.16	77	1	I
1530-C1-V2	22.24	180.16	82	1	I
1530-C1-V3	59.85	186.37	84	2e	II
1530-C1-V4	271.41	200.74	68	5	II
1530-C1-V5	309.46	190.42	67	5	II
1530-C1-V6	314.18	182.34	78	5	V

Table 4.5

Distribution of fractures and veins at Site U1530 grouped by lithology and alteration type.

Lithology	Alteration Type	Fracture Total	% Fractures in Site	Vein Total	% Veins in Site	% Planar Features in Site
1	I	2	2.50	27	6.84	6.11
2	II	8	10.00	36	9.11	9.26
3	II	3	3.75	27	6.84	6.32
4	II	0	0.00	9	2.28	1.89
4	IIIa	4	5.00	10	2.53	2.95
4	IIIb	4	5.00	13	3.29	3.58
4	IV	14	17.50	19	4.81	6.95
5	II	11	13.75	86	21.77	20.42
5	IV	18	22.50	55	13.92	15.37
5	V	16	20.00	113	28.61	27.16

4.1.4 Site U1528

Site U1528 has more fractures that were re-oriented (n=77) than Site U1530 but significantly less reoriented veins. Only 2 fractures have a dip magnitude of <10°, with the majority of dips having moderate-to-high values (Figure 4.4). A total of 6 veins and 1 fracture can be seen in the central cluster, which includes the shallow-dipping features (Fig. 4.4; Table 4.6). Dip direction is less variable, with small clusters dipping ENE or

WSW. These clusters are made of 10 veins, most of which occur between 200-300 mbsf
(Table 4.7). There is another notable clustering of NNE or SSW dipping planar features
that is observed at Site U1528. This NNE or SSW moderately dipping cluster is
comprised of 15 veins and 1 fracture (Table 4.8). The total fractures and veins at Site
U1527 and their distribution among different lithologies and alteration types are listed
below (Table 4.9).
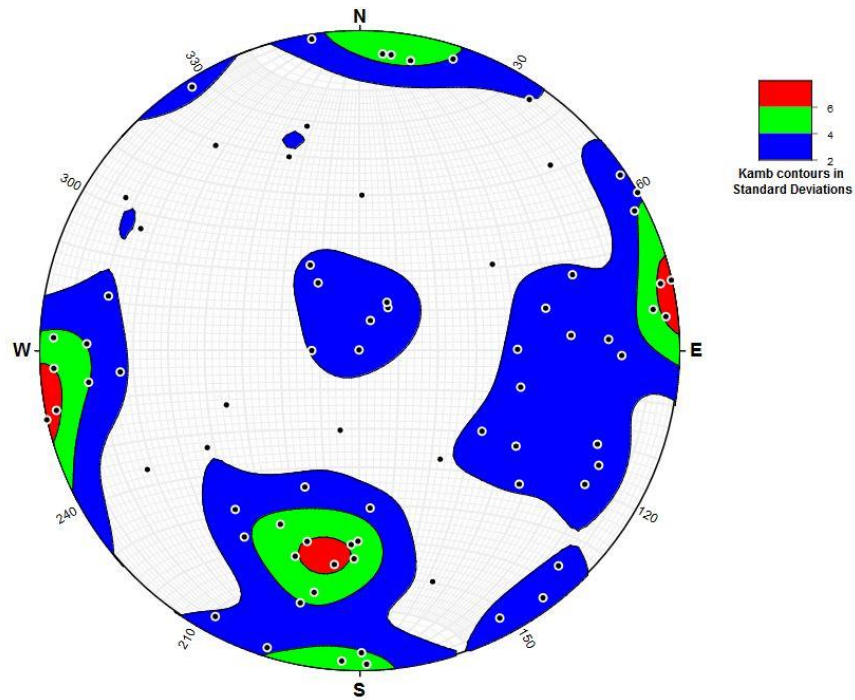
Figure 4.4

Poles to planes of fractures and veins at Site U1528.

Table 4.6

Reoriented shallow dipping features (central cluster) at Site U1528.

Fracture/Vein ID	Depth (mbsf)	Azimuthal Orientation (degrees)	Dip Magnitude (degrees)	Igneous Unit	Alteration Type
1528-C1-V1	66.56	148.61	20	2a	III
1528- C1-F1	221.11	200.97	8	2c	III
1528- C1-V2	258.69	150.09	25	2c	III
1528- C1-V3	283.26	214.29	13	3	II
1528- C1-V4	283.70	089.29	12	3	II
1528- C1-V5	289.78	004.48	0	3	III
1528- C1-V6	302.01	210.32	14	3	III

Table 4.7

Reoriented features located in the ENE or WSW dipping clusters at Site U1528.

Fracture/Vein ID	Depth (mbsf)	Azimuthal Orientation (degrees)	Dip Magnitude (degrees)	Igneous Unit	Alteration Type
1528- C1-V7	110.67	078.71	86	2a	II
1528- C1-V8	192.80	091.29	74	2c	II
1528- C1-V9	207.30	083.19	74	2c	II
1528- C1-V10	212.73	257.59	86	2c	III
1528- C1-V11	225.17	257.39	90	2c	III
1528- C1-V12	225.17	077.39	90	2c	III
1528- C1-V13	289.16	263.80	86	3	III
1528- C1-V14	297.34	262.15	82	3	II
1528- C1-V15	304.12	086.55	85	3	III
1528- C1-V16	344.90	092.29	85	3	II

Table 4.8

Reoriented features located in the NNE or SSW dipping clusters at Site U1528.

Fracture/Vein ID	Depth (mbsf)	Azimuthal Orientation (degrees)	Dip Magnitude (degrees)	Igneous Unit	Alteration Type
1528- C2-F2	114.83	010.51	66	2a	II
1528- C2-V17	191.46	359.53	84	2c	II
1528- C2-V18	207.30	015.16	52	2c	II
1528- C2-V19	254.69	0186.20	82	2c	III
1528- C2-V20	258.70	013.09	70	2c	III
1528- C2-V21	258.70	190.09	81	2c	III
1528- C2-V22	264.39	197.91	85	2c	III
1528- C2-V23	273.27	001.38	55	2c	II
1528- C2-V24	283.09	017.22	57	3	II
1528- C2-V25	283.70	024.29	50	3	II
1528- C2-V26	298.12	006.58	57	3	II
1528- C2-V27	301.92	002.32	51	3	III
1528- C2-V28	302.07	000.32	50	3	III
1528- C2-V29	304.15	184.55	82	3	III
1528- C2-V30	311.39	358.61	88	3	II
1528- C2-V31	330.73	003.2	87	3	III

Table 4.9

Distribution of fractures and veins at Site U1528 grouped by lithology and alteration

type.

Lithology	Alteration Type	Fracture Total	% Fractures in Site	Vein Total	% Veins in Site	% Planar Features in Site
2a	I	0	0.00	2	0.39	0.35
2a	II	16	29.63	52	10.18	12.04
2a	III	15	27.78	93	18.20	19.12
2b	II	2	3.70	5	0.98	1.24
2b	III	5	9.26	0	0.00	0.88
2c	II	6	11.11	101	19.77	18.94
2c	III	3	5.56	108	21.14	19.65
3	II	2	3.70	67	13.11	12.21
3	III	5	9.26	83	16.24	15.58

4.2 Downhole Correlation

4.2.1 Site U1527

     A total of 303 depth bins were described at Site U1527. The data used for this

analysis is from Holes U1527A and U1527C, which was compiled to produce a singular

composite hole. The results of the correlation for Site U1527 can be seen below (Table

4.10). DVTZ is omitted from this site given the lack of discrete veins present in either

hole. There is a moderately strong positive correlation between LithZ and AltZ. FDZ

and DFTZ show a weakly positive correlation. FDZ shares a weak negative correlation

with both LithZ and AltZ. All other variables correlations are very weak.

Table 4.10

Heat-map of correlations among characteristics at Site U1527.

	VDZ	*FDZ*	*LithZ*	*AltZ*	*DFTZ*
VDZ	1				
FDZ	-0.00534	1			
LithZ	-0.02587	-0.39182	1		
AltZ	0.09418	-0.33377	0.577924	1	
DFTZ	0.063635	0.330374	0.069133	0.039662	1

4.2.2 Site U1530

A total 867 values were collected for each variable at Site U1530. The values were taken from core in Hole U1530A. Below is the result of the correlation analysis for Site U1530 (Table 4.11). There is a very strong correlation between the two fracture variables, FDZ and DFTZ. All other variables at Site U1530 show very weak correlation to one another, although the positive relationship of VDZ and DVTZ, as well as the negative relationship between LithZ and DVTZ, have higher absolute values than the rest.

Table 4.11

Heat-map of correlations among characteristics at Site U1530.

	VDZ	FDZ	LithZ	AltZ	DVTZ	DFTZ
VDZ	1					
FDZ	-0.05308	1				
LithZ	-0.04049	0.005818	1			
AltZ	0.044194	0.010429	-0.05304	1		
DVTZ	0.129904	0.047985	-0.18527	0.019487	1	
DFTZ	-0.01882	0.811402	0.008099	0.009315	0.099995	1

4.2.3 Site 1528

A total 1194 values were collected for each variable at Site U1528. The values were taken from core in Holes U1528A and U1528D, which were used to create a singular composite hole for analysis. The result of the correlation analysis for Site U1528 is show below (Table 4.12). VDZ has a very weak positive relationship to AltZ and DVTZ; with LithZ, VDZ has a weak positive relationship. FDZ and DFTZ share a strong positive correlation. LithZ also shares a very weak positive relationship to AltZ and DVTZ. All other variables show a very weak correlation.

Table 4.12

	VDZ	FDZ	LithZ	AltZ	DVTZ	DFTZ
VDZ	1					
FDZ	-0.04509	1				
LithZ	0.224999	0.008069	1			
AltZ	0.140905	-0.00144	0.110804	1		
DVTZ	0.176913	-0.04138	0.143616	0.026964	1	
DFTZ	0.004193	0.649576	0.019717	-0.00302	-0.06156	1

4.3 Thin Section Analysis

4.3.1 Site U1527

Hole U1527C (Table 6.1) contains five total veins seen in thin section observation. Quartz is the dominant mineral fill of all five veins, with two accompanying unknown clay minerals: UCM1, a white clay mineral that appears blue-to-yellow in cross polarized light (XPL), and UCM2, another white clay mineral that appears green-to-yellow in XPL. In sample 1527C-13R-2-107-111 cm, a single quartz vein (V27-1) was observed with no visible growth orientation. Three sub-parallel veins present in sample 1527C-17R-2-53-58 cm contain quartz displaying up-core growth perpendicular to the host rock walls without a visible median suture, whereas another vein in the same thin section shows no visible growth orientation. All veins in sample 1527C-17R-2-53-58 cm contain UCM2 and pyrite. Additionally, all veins observed in thin section at Site U1527 occur in lithologic unit 2b and alteration type IIa, as defined in the ship report (Table 6.2) (de Ronde et al., 2019).

4.3.2 Site U1530

HoleU1530A contains 14 veins seen in thin section observation with quartz and UCM1 as the primary mineral fill (Table 6.3). The corresponding lithologies hosting these veins are also reported (Table 6.4). Accompanying minerals include gypsum, anhydrite, pyrite, and UCM2. In sample 1530A-12R-1-109-113 cm, two veins can be seen intersecting. The older vein contains quartz and pyrite, with the quartz grains having grown perpendicular to the vein wall with a median suture. The older vein shows

up-core growth, similar to the set of three veins observed in Hole 1527C. The younger

vein contains quartz, anhydrite, and gypsum, with no visible growth orientation. The

younger vein also has another vein sub-parallel beside it with the same mineral fill, with

the vein dipping approximately NE. A vug is present in the younger vein with the same

mineral fill as the vein.

Four veins were observed in sample 1530A-50R-1-48-50 cm, all containing

quartz and UCM1 as their fill. Visible growth orientation was not observed in any of the

four veins, and the rightmost two veins had poorly defined boundaries. All four veins

exhibit a pattern of finer-grained minerals on the edges of the veins, bounding the

coarser-grained minerals. The intersection of these four veins is a sub-circular area of

quartz and UCM1.

Sample 1530A-50R-1-56-58 cm contains two veins. The uppermost, sub-

horizontal vein is filled with anhedral quartz and UCM1, showing no visible growth

orientation. The lowermost, sub-vertical vein is almost entirely filled with UCM1; a

significantly lower abundance of quartz was observed in this vein when compared to the

neighboring vein. The UCM1 in a sub-vertical vein varied in size, including larger

crystals. A single vein filled with UCM1 was seen in sample 1530A-53R-1-13-15 cm.

This vein contains low amounts of pyrite, although the surrounding host rock contains

abundant scattered pyrite.

In sample 1530A-55R-2-4-7 cm, a single vein containing quartz and UCM1 was

observed. The clay in the vein showed sub-horizontal growth orientation with no

identifiable median suture. In addition, the growth orientation of the clay was only

observed in three areas in the vein, which did not best represent the overall appearance of

clay in the vein. The surrounding host rock contains relatively thinner veins (compared to the aforementioned vein in this sample) of pyrite, even though pyrite was absent in the vein.

Sample 1530A-60R-1-54-56 cm contains a vein of subhedral-to-euhedral quartz and pyrite, with the pyrite confined to the downcore wall of the vein. This vein does not show visible growth orientation; the euhedral quartz appears to have grown in a multitude of directions. A blue discoloration was observed on the quartz, likely from thin section preparation. In the center of the thin section, an area of highly concentrated pyrite was observed. There were no veins observed connecting this area to the rest of the thin section.

In sample 1530A-75R-1-68-71 cm, a relatively large sub-vertical vein (1-8mm thick.) displays medium-to-coarse grained anhydrite (Figure 4.5). The vein contains minimal pyrite, while the surrounding host rock contained a high amount of pyrite. The anhydrite in the vein, verified by EDS, displays no visible growth orientation, as the grains are anhedral and blocky.

Sample 1530A-88R-1-24-26 cm shows a single sub-horizontal vein containing almost 100% pyrite (Figure 9). The vein contains minor amounts of quartz, UCM1, and UCM2. There are thinner veins nearby that contain quartz, pyrite, and UCM1. Some of these veins show median sutures between quartz grains, but not consistently. The larger pyrite vein forms across the quartz veins, going from discrete to diffuse up-core. The pyrite appears to have formed after the quartz filled the vein, making it the younger of the two.
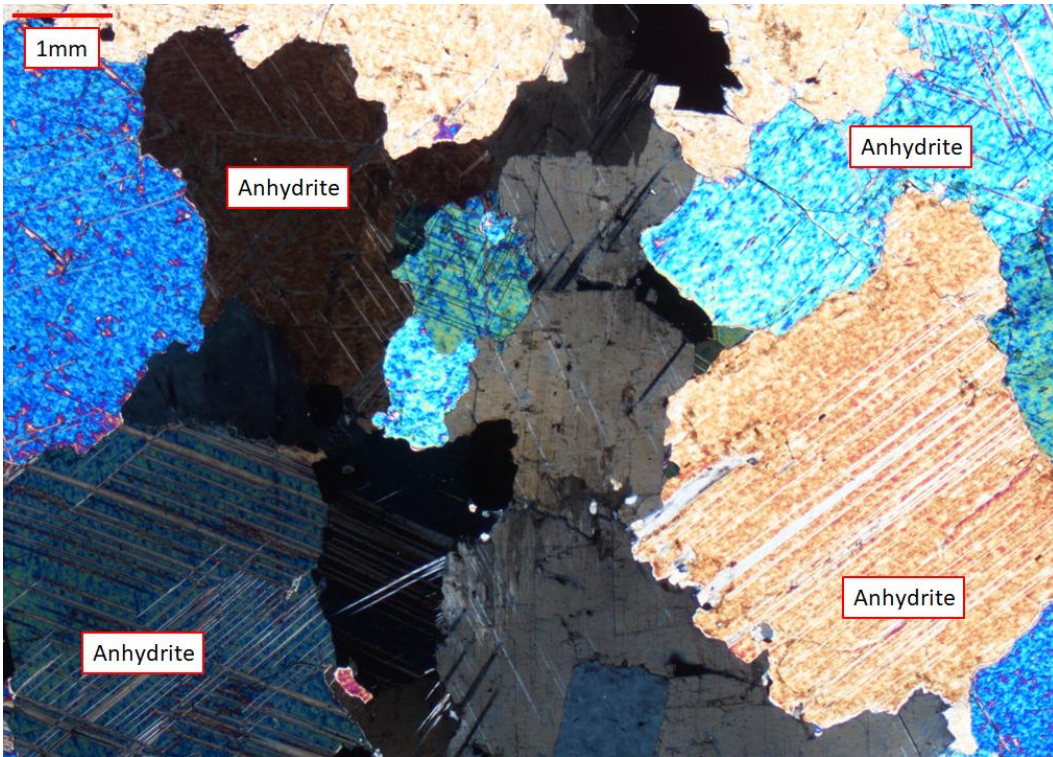
Figure 4.5

Blocky anhydrite in Hole U1530A.
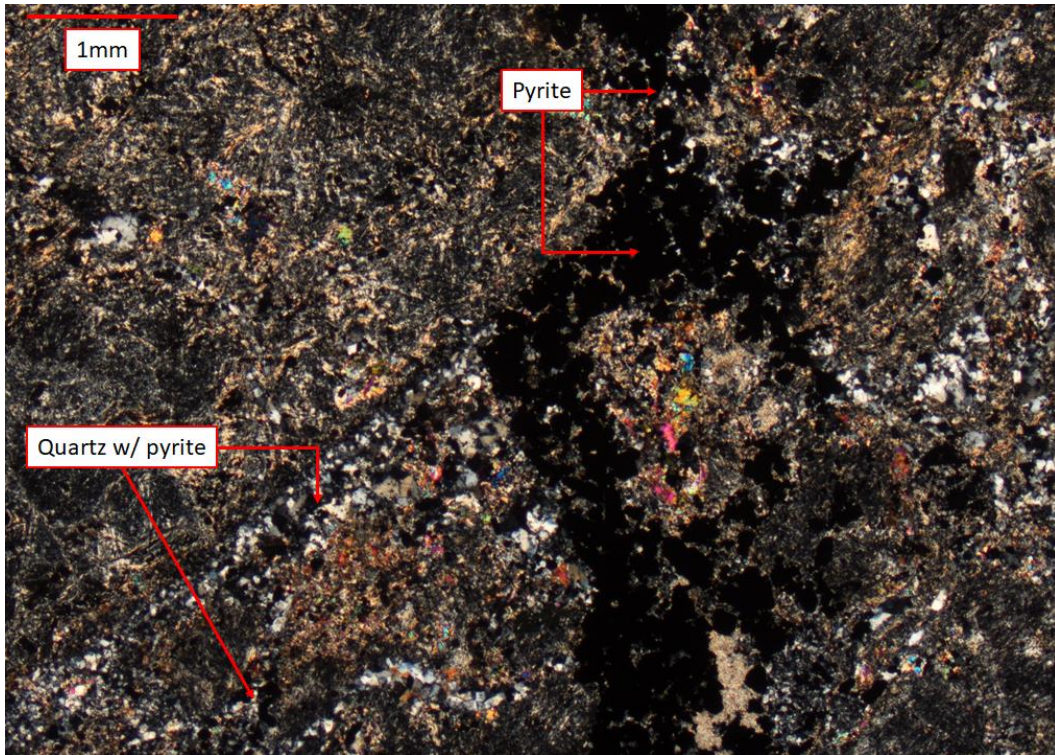
Figure 4.6

Quartz overgrown with pyrite in Hole U1530A.

4.3.3 Site U1528

Hole U1528A (Table 6.5, 6.6) contains five veins viewed in thin section with quartz and anhydrite as dominant mineral fill, with accompanying gypsum, pyrite, UCM1, and UCM2. A single vein observed in sample 1528A-8R-1-52-54 cm containing quartz and UCM1 shows no visible growth orientation. In sample 1528A-9R-2-70-75 cm, a single vein was observed having dominant gypsum and anhydrite, with accompanying minor quartz and UCM2. The aforementioned vein does not show visible growth orientation.

Sample 1528A-9R-3-2-4 cm contains a sideways Y-shaped vein, which is described as having two "branches" and a "trunk" (Figure 4.7). The younger, uppermost "branch" vein (2, Fig 4.7) contains gypsum, pyrite, UCM1, and UCM2. The vein does

49

not show visible growth orientation. The older, lowermost "branch" vein (1, Fig. 4.7)

contains the same fill, although there is notably less UCM1 occupying the vein. The

older vein does not contain UCM2 as seen in the other vein present in this sample. The

older vein also fails to show visible growth orientation. The "trunk" vein (3, Fig. 4.7)

contains the same mineral fill of the uppermost vein, and also includes two coarser-

grained crystals of native sulfur (identified through EDS analysis) (Figure 4.8). The

"trunk" vein does not show visible growth orientation.
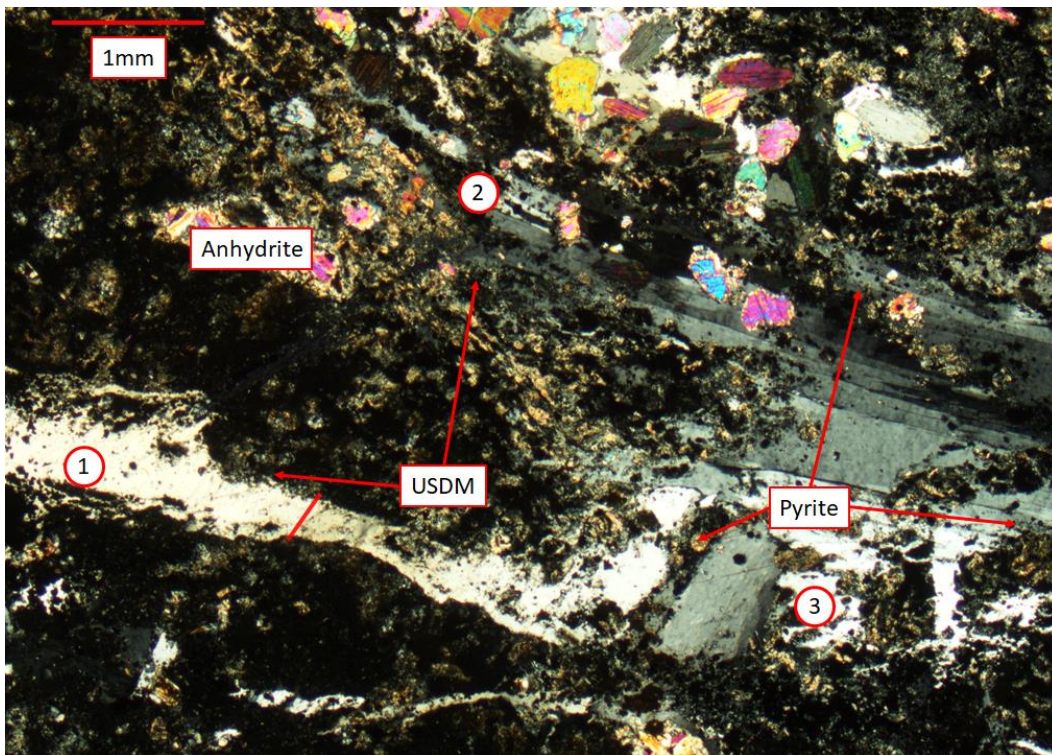
Figure 4.7

Y-shape branch in Hole 1528A showing an older vein (1) and a younger vein (2) that have split from each other. The "trunk" of this Y-shape (3) shares the same mineral fill as the younger vein.
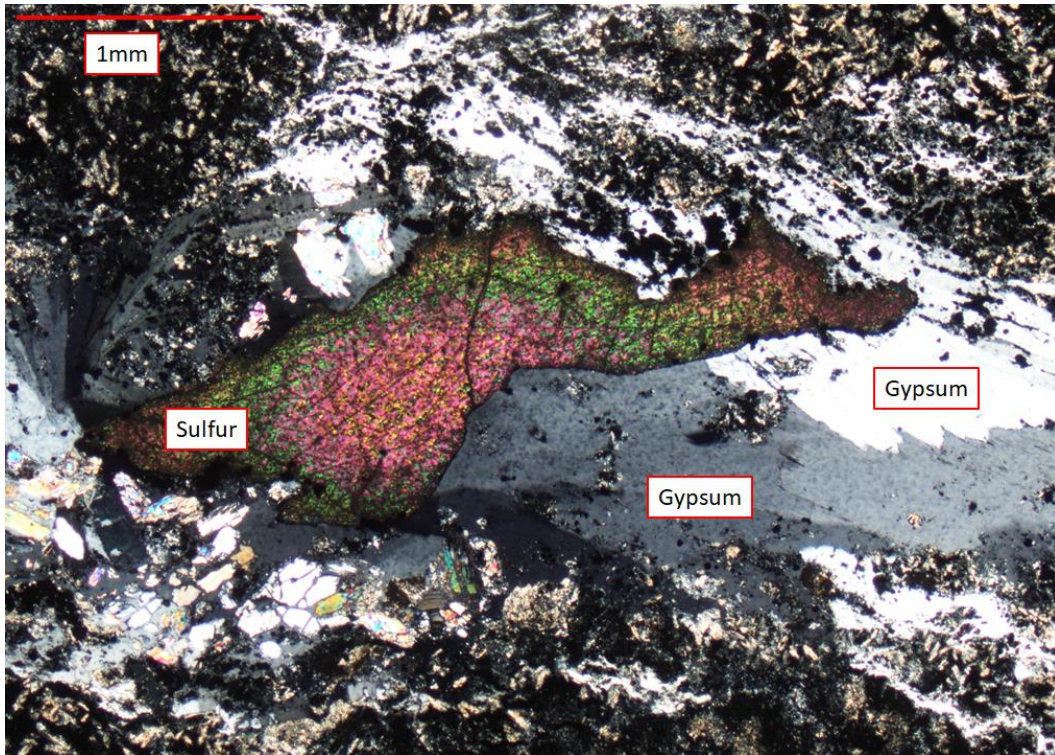
Figure 4.8

A grain of native sulfur found in Hole 1528A.

Hole U1528D contains 19 veins viewed in thin section with predominantly anhydrite and gypsum fill, although quartz is in veins that are more up-core (Table 6.7, 6.8). Minor accompanying minerals include pyrite, UCM1, UCM2, and an unknown silica dioxide mineral (USDM). In sample 1528D-9R-1-95-97 cm, three veins were observed. Two of these veins contain quartz and anhydrite both occupying approximately equal space. The third vein is mainly quartz, with accompanying pyrite and UCM1. No veins observed in this section show visible growth orientation.

Two veins were observed in sample 1528D-14R-1-74-79 cm with anhydrite mineral fill. The longer of the veins shows a possible anhydrite median suture, albeit poorly-defined. This vein also contains minor quartz and shows an increasing amount of

pyrite down-core. The shorter vein at this depth range has a primarily anhydrite fill, with minor quartz and pyrite. This vein does not show visible growth orientation. Within sample 1528D-21R-2-61-66 cm, a well-defined vein of anhydrite and pyrite is observed, with no visible growth orientation. Above and below this vein, a networked area of thinner, finer-grained anhydrite can be observed, with pyrite also found in the lower area. These networked veins do not have well defined boundaries and fail to show visible growth orientation.

In sample 1528D-34R-1-127-129 cm, an intersection of two veins was observed (Figure 4.9). A sub-vertical vein contains anhydrite perpendicular to the vein wall with no observable median suture, along with minimal pyrite in the up-core portion. Down-core, the aforementioned sub-vertical vein contains randomly oriented anhydrite crystals and noticeably more pyrite than the up-core portion. A sub-horizontal vein contains blocky, randomly oriented anhydrite on either side of the intersection.

Four veins were observed in sample 1528D-39R-1-17-21 cm; anhydrite and pyrite were observed in all, with no visible growth orientation. An intersection of three relatively smaller veins in that depth resulted in a vug containing the same minerals as the veins.

In sample 1528D-43R-1-18-21 cm, an intersection of two veins was observed, both with a haloed area around the veins indicated by an absence of pyrite in the host rock. Pyrite was observed on the outside of the halo in relatively high amounts. The older vein, which is noticeably longer with poorly defined boundaries, contains anhydrite, minimal pyrite, and UCM1. The younger vein in this zone has well defined boundaries

52

and contains the same fill as the older vein. Both veins lack visible fiber growth orientation.

Sample 1528D-51R-2-27-30 cm contains two sub-vertical veins observed with tip ends in close proximity. One vein contains a linear alignment of pyrite in the center of the vein, bordered on either side by gypsum that is aligned perpendicular to the wall (sub-horizontal to up-core) without a median suture. The other vein is primarily finer-grained gypsum and anhydrite, with no visible growth orientation.

Three veins were observed in sample 1528D-55R-1-39-42 cm, all containing anhydrite and pyrite, with no visible growth orientation. The rightmost down-core vein shows a possible, poorly-defined median suture of larger anhydrite grains next to finer-grained anhydrite. This vein also contains USDM (Figure 4.10). The leftmost downcore vein contains anhydrite, gypsum, and pyrite, with a section of larger anhydrite grains next to finer-grained anhydrite. The observed up-core vein contains finer-grained anhydrite and pyrite, and cuts across plagioclase grains in the host rock.
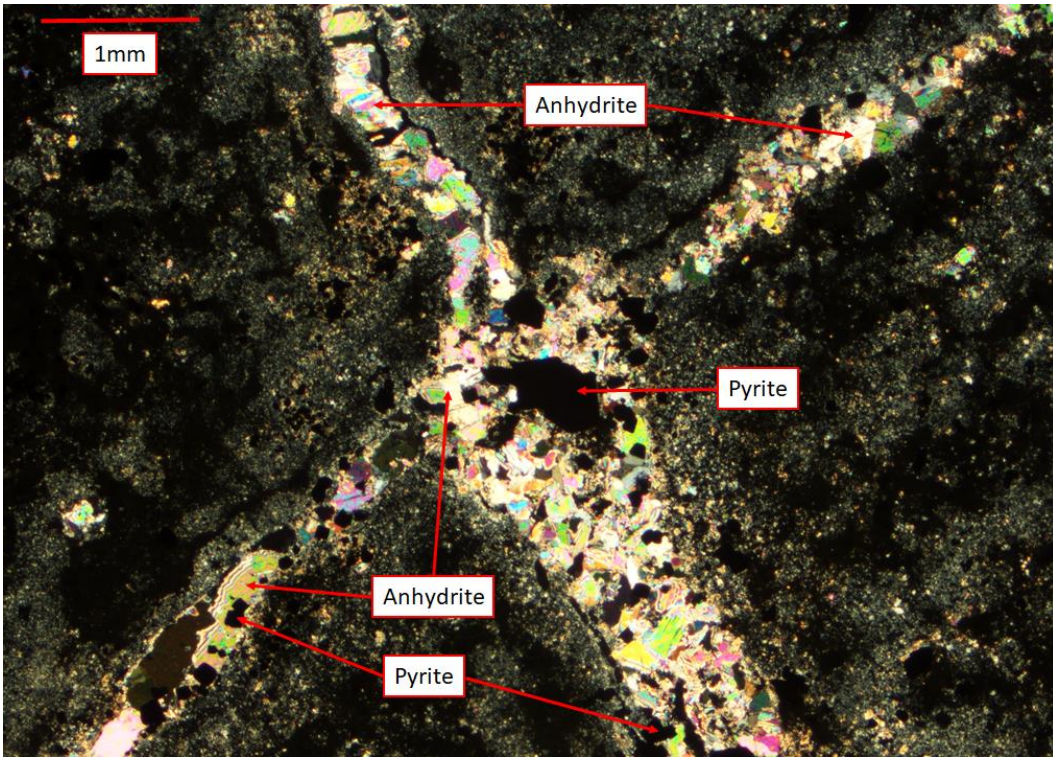
Figure 4.9

An intersection of two veins in Hole U1528D. Both veins contain the same mineral fill, although pyrite is largely confined to the two downcore vein ends.
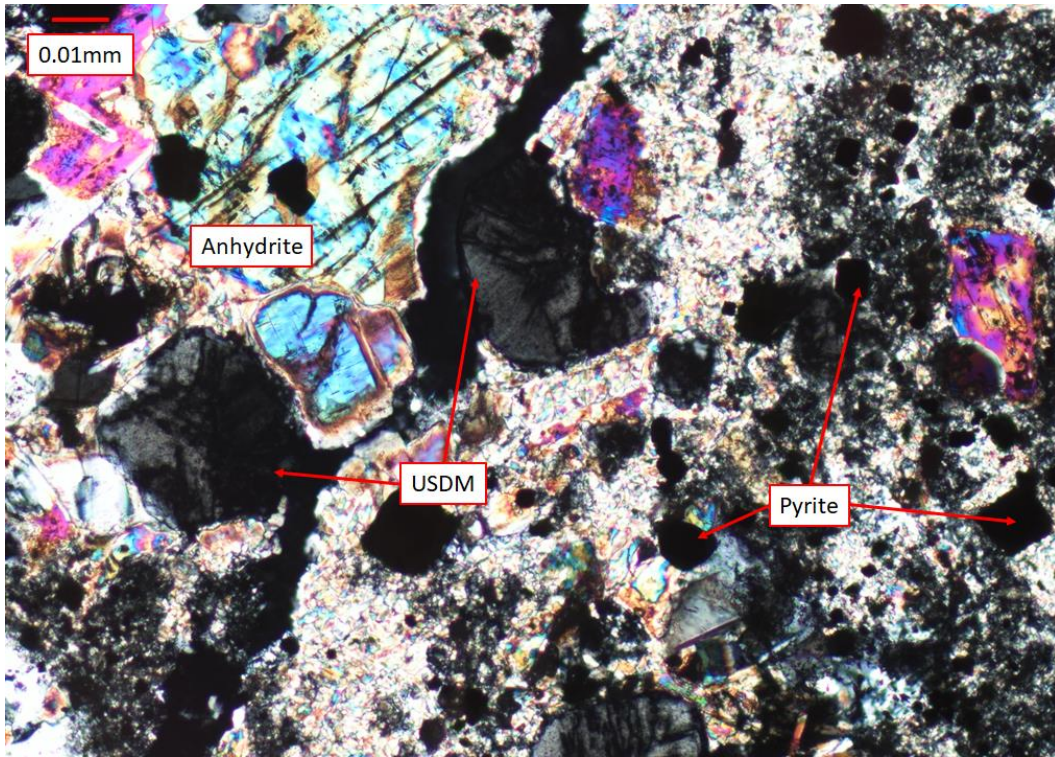
Figure 4.10

USDM observed in Hole U1528D.

4.3.4 Thin Section Summary

For all three sites, six of the 43 veins (14%) observed in thin sections display orientated mineral fibers. Of those six veins, two showed mineral fibers with a sub-horizontal alignment. The four remaining veins showed up-core mineral growth. The most common mineral fill of oriented fibers is quartz (n=4), with anhydrite and gypsum filling the other two veins. Five of the six veins with mineral fiber orientation occur in the 200-300 mbsf interval of each hole, with one vein being in the 60-70 mbsf range. The lithology shows that reoriented veins appear in both altered volcaniclastic rocks and altered dacite, with a slight preference to the altered volcaniclastic rocks (Table 6.9). Alteration type II, and the subtypes thereof, is the most common alteration type among the veins with mineral fiber orientation (Table 6.9).

CHAPTER V – DISCUSSION

This caldera-wide study focuses on the paleomagnetic reorientation of discrete fractures and veins, downcore correlation of key characteristics such as lithology and alteration type, and thin section observations. For this discussion, recall the stress field of the region: σ_1 is vertical, σ_2 is approximately NE-SW and sub-horizontal, and σ_3 is approximately NW-SE, direction of regional extension, and sub-horizontal (Anderson, 1951; Lipman, 1997; Embley et al., 2012). In the following section, the main results presented above will be explained and an overall model of fluid pathways will be presented. The study of paleomagnetic realigned fractures and veins seeks to constrain the regional controls on brittle feature generation, while examining each site individually to identify the potential for local controls. The main factors of control in question are regional extension, caldera collapse, and fluid overpressure. Downcore linear regression aims to identify correlations among one or more key characteristics at each site to determine if any combination of factors leads to enhanced or inhibited fluid movement. Recent studies suggest that rock strength, which is not directly mentioned in this study, declines as porosity increases (Heap et al., 2021). This may account for disparities in brittle features between the two main lithologies, which is detailed below. Thin section observation provides insight on fracture generation methods by examining mineral fiber growth, while also comparing mineral fill to look for changes in source fluids or evidence of reopening/cross-cutting relationship to determine relative age of fluid movement in the caldera.

5.1 Paleomagnetic Core Realignment

5.1.1 Volcano-wide Results

Regional extension may cause mode I fractures (joints, opening) to form that open parallel to the extensional direction (Hancock et al., 1984). In the case of Brothers volcano, these fractures would strike approximately ENE-WSW, given the regional extension is WNW-ESE (Wright, 1994). These fractures may also appear as conjugate pairs, with dip direction toward either the NW or SE. However, the results here show the poles-to-planes projection of fractures and veins on a volcano-wide scale produces a stereonet with widely scattered points (Fig. 4.1). The high variance in fracture/vein orientation is likely due to the fact that many generations of extension are recorded. It must also be kept in mind that fluid overpressure or caldera-collapse generated fractures may have orientation similar to that of regional extension, and therefore may be grouped in datasets that appear to be associated with regional extension. Furthermore, fractures generated by fluid overpressure or caldera collapse may also appear sub-vertical and strike perpendicular to σ_3, thereby making it hard to differentiate them on a stereonet (Secor, 1965). The sub-population of fractures and veins that have an attitude that matches those predicted to form by regional extension are interpreted to form from those causes; however, other local processes are likely needed to explain the other populations and are discussed below.

58

5.1.2 Sites U1527 and U1530: Caldera Wall

Reoriented fractures from Site U1527 were few (n=10), but there is a generalized clustering of poles-to-planes on the NNW and SSE directions (Fig. 4.2). Given that the dip of these fractures is parallel to σ_3, there is the possibility that they form a conjugate set and are associated with extensional regional tectonics during caldera formation (Lipman, 1997; Embley et al., 2012). Piston-like collapse was proposed as one possible way the Brothers volcano caldera formed (Wright and Gamble, 1999). Piston-like collapse would show continuous ring-faulting around the caldera wall (Lipman, 1997). An obvious continuous ring-fault is not present in Brothers volcano, but steep scarps instead may be related to caldera formation (Lipman 1997; Embley et al., 2012). It is therefore unlikely that the fractures seen at Site U1527 are from piston-like caldera collapse. If the collapse was asymmetric (trap door) as proposed by Embley et al. (2012), the ring-fault would only be partially observed. In the case of Brothers volcano, the ring-fault is observed on the NW wall, where the caldera floor is topographically lower than the SW portion of the caldera (Embley et al., 2012). It is therefore likely that higher-angle, outward-dipping (NW) fractures on the NW wall seen in stereonet projection from Site U1527 are associated with the down-sagged end of an asymmetrical collapse (Fig. 4.2, 4.3). There was no evidence at Sites U1527 or U1530 of reverse faulting (de Ronde et al., 2019a), so it is unlikely that inward-dipping (SE) fractures are similar to those seen in experimental studies (Acocella et al., 2000). Instead, it may be that these SE-dipping fractures are part of a conjugate set with the NW-dipping fractures

and thereby related to regional extension; however, fluid overpressure and caldera collapse could also be the cause.

The majority of fractures and veins at Site U1527 (including veins that could not be measured for dip magnitude/direction) occur in two volcaniclastic lithologic units: 2b (pervasively altered, matrix-supported, poorly sorted lapilli-tuff, lapillistone, and tuff-breccia) and 2d (altered matrix- and clast-supported lapilli-tuffs and class-supported tuff-breccias) (de Ronde et al., 2019a). Additionally, the lithologies hosting these planar features fall under alteration type IIa classification (highly altered with abundant chlorite, quartz, illite, and smectite, with minor mordenite) (de Ronde et al., 2019a). Host lithology of nearly all fractures and veins at Site U1527 is described as highly altered, with individual dacite clasts detailed as slightly-to-highly altered (de Ronde et al., 2019a). Only fractures and veins found at shallower depths are in lithologies described as slightly altered (de Ronde et al., 2019a). Given that both lithologies are volcaniclastic, the variability of alteration intensity may be accounted for by factoring in time. The shallower volcaniclastics are younger (de Ronde et al., 2019a), which may mean they have simply had less time to be altered. The alteration intensity differences could also be reflected by the fracture/vein total in those lithologies; the older volcaniclastics have a greater total number of brittle features that would allow for the movement of fluids and subsequent increased alteration. This may also indicate that the older units have had longer to become fractured and veined. Another possibility is that fluids take a preferred pathway toward hydrothermal vents, and subsequently limit the overall effective alteration of the host lithology. A preferred pathway may also explain the higher abundance of fractures and veins in older, deeper rocks: as fluids move closer to the

seafloor, they migrate from a wider, more diverse network (with a goal of ascension) to a more confined network that focuses on venting.

Site U1530 notably has several shallow dipping planar features, which contrasts with the lack thereof at Site U1527 (Fig. 4.3). Given that σ_1 is approximately vertical while σ_2 and σ_3 are on in horizontal plane, it is not expected that horizontal fractures would form as a result of regional tectonics. Additionally, the overburden would work to close any sub-horizontal features. Hubbert et al. (1957) states that horizontal fractures should only form where the total fluid pressure is greater than total vertical pressure. This suggests that horizontal fractures likely involve fluids, and are not likely related to tectonic processes. Two factors must then be considered: either the fluid pressure is increased to generate the horizontal fracture, or the vertical pressure is decreased. As seen in the downhole correlation results (discussion below), there is no correlation between fracture/vein density and lithology at Site U1530 where the horizontal fractures are observed. For Site U1530, it is likely that sub-horizontal veins are a result of decreased vertical pressure. A decrease in vertical pressure from above could be possible in the form of mass wasting events, but it may not be significant enough to allow sub-horizontal vein creation. Vertical pressure would then need to decrease from below in order to allow horizontal fracturing to occur. One possible method for this is caldera down-drop, where the emptying of a magma chamber after eruption removes the pressure from inside the volcano, allowing for collapse (Lipman, 1997; Acocella et al., 2000; Stix et al., 2003). If the stress on σ_1 (vertical) is less than σ_2 or σ_3 (both horizontal) during down-drop, it would be possible for horizontal fractures and veins to form.

Fractures and veins from the total dataset at Site U1530 are most common in

lithologic unit 5 (altered volcanic rock with intercalated altered plagioclase-phyric lava)

and alteration types II (intensely altered with abundant quartz, illite, and chlorite; the

chlorite gives it a characteristic green color) and V (intensely altered with diaspore,

quartz, pyrophyllite, smectite, and rutile with a characteristic buff-brown color) (de

Ronde et al., 2019a). All lithologies at Site U1530 are described in the ship report as

intensely altered (de Ronde et al, 2019a). However, there is no correlation that appears in

the linear regression study (discussion below) to suggest that alteration intensity plays a

significant role in fracture and vein propagation through the dacite lava flows. This may

be because all lithologies are described as highly or intensely altered so the correlation is

lost.

5.1.3 Site U1528: Resurgent Cone

A set of planar features dipping ENE or WSW can be seen on the stereonet, as

well as a NNE or SSW dipping set (Fig. 4.4). Both sets are moderate-to-steeply dipping.

It is possible that these planar features are associated with rising magma at the resurgent

cone, which generates fractures in a ring-like pattern due to uplift from the underlying

magma (Acocella et al., 2000). Fractures and veins at Site U1528 occur in both lithologic

units 2 and 3. Lithologic unit 2 includes subtypes 2a and 2c, which are volcaniclastics

rocks, whereas subtype 2b is a dacite lava flow (de Ronde et al., 2019a). Lithologic unit

3 is described as a dacite lava flow, although distinct enough to separate it from lithologic

unit 2b (de Ronde et al., 2019a). Both units are described as highly-to-intensely altered

(de Ronde et al., 2019a). The lack of discrete fractures and veins in subunit 2b may

reflect that the fluid pressure was not strong enough to easily penetrate the dacite lava flow. However the fluids would be able to move through the volcaniclastic rocks, as indicated by the abundance of brittle features in these units. Alteration intensity shares a very weak positive correlation with lithology, so it is unlikely that the degree of alteration influences the lithologic susceptibility of fracture and vein penetration. As mentioned previously, the overall state of alteration may cause a loss of strength between these correlations. There are also sub-horizontal veins that appear at Site U1528. At Sites U1527 and U1530, sub-horizontal veins were suggested to have formed via caldera down-drop (see above); at Site U1528, that may not be the case. Recall that for sub-horizontal veins to form, there must either be an increase in fluid pressure strong enough to surpass the stress in the σ_1 direction or a decrease in stress in the σ_1 direction. Since Site U1528 is located on the resurgent cone (de Ronde et al., 2011), it is unlikely that there is a decrease in σ_1 stress from underneath (previously associated with a deflating magma chamber). The magma chamber has refilled to some extent, and thus may have caused uplift which generates upward stress in the σ_1 direction. As the magma chamber cycled between filling and emptying during eruptions, there may have been brief periods of time where sub-horizontal fractures could have formed. Therefore, fluid pressure likely increased to generate the sub-horizontal fractures and created the sub-horizontal features seen at Site U1528 (Phillips, 1972; Bons et al., 2012; Cucci et al., 2016).

Heap (2021) suggests that porous rocks are lower in strength than non-porous rocks. The strength of volcanic rocks decreases as porosity increases (Al-Harthi et al., 1999; Heap et al., 2021), and volcaniclastic rocks and sedimentary rocks (igneous units 4 and 2, respectively) are more porous than the dacite lava flows (de Ronde et al., 2019a).

Other literature that suggests high alteration intensity leads to a decrease in lithologic integrity (Mordensky et al., 2018). At Brothers volcano, the volcaniclastic rocks would be more susceptible to fluid movement than the dacite lava flows. Perhaps the fluids ascended through volcaniclastic rocks until they met resistance at an overlying dacite lava flows. At this point, fluid could move laterally through the volcaniclastic rocks, creating vein networks that reflect the high vein density seen in the linear regression study below. Over time, episodic events could generate fluid pressure strong enough to fracture the dacite lava flows, allowing for repetition of this pattern as the lithology continues to alternate upward. This could then account for the sub-horizontal veins seen throughout multiple depth intervals at Site U1528.

5.2 Downhole Correlation

There is a moderately strong positive correlation between lithology and alteration intensity at Site U1527. This matches what is seen on the shipboard alteration intensity plot (de Ronde et al., 2019a). Furthermore, approximately 83% of the fractures and 100% of the veins occur in igneous unit 2 at Site U1527. For alteration type, approximately 66% of the fractures and 100% of the veins occur in alteration type II (including subtypes IIa and IIb). The moderately strong positive correlation and the distribution of planar features may suggest that volcaniclastic units are more susceptible to fracturing and fluid flow due to increased fracture-related permeability, and therefore may experience a higher degree of alteration.

Another weakly positive correlation exists between fracture density and discrete fracture total. This correlation simply implies that the presence of measurable fractures

increases as the overall fracture density increases. Fracture density shares a weak negative correlation with both lithology and alteration intensity. Such a relationship between fracture density and lithology implies that fractures are more likely to appear less frequently in certain lithologies. Reviewing the data from the Site U1527 paleomagnetic study, igneous unit 1 appears to show a much lower density of fractures than igneous unit 2. This may be because igneous unit 1 is younger and has not had as much time to allow fluid interaction or fracture generation compared to igneous unit 2. The weak negative relationship between fracture density and alteration intensity suggests that fractures are less dense in highly altered rocks. This may be because increased alteration causes fractures to be destroyed as lithologic integrity is lost.

Site U1530 does not show all the same correlations as Site U1527. Again, due to their location on the caldera wall and similar hydrothermal fluid types (de Ronde et al., 2019), similarities between the two sites would be expected. Site U1530 does display a very strong positive correlation between fracture density and discrete fracture total, but that is to be expected. Site U1530 shows a weakly negative correlation between lithology and discrete vein total. This may suggest that certain lithologies host a larger total of discrete veins, which could reflect volcaniclastic lithologies hosting more network veins and volcanic lava flow layers having more discrete veins. Indeed, 55% of the reoriented (discrete) veins are seen in dacite lava flows. A very weak negative correlation does exist between lithology and vein density, which indicates that some lithologies have a more prominent presence of network veins. At Site U1530, the mean porosity of the volcaniclastic rocks is 59% volume, where as in the dacite lava flows the mean porosity is 21% volume (de Ronde et al., 2019a). It would therefore follow that the volcaniclastic

rocks would be more suitable for hosting vein networks. Fracture and vein density both show a positive relation with alteration intensity, and although alteration does weaken the host rock (Mordensky et al., 2018), all units at Site U1530 except lithologic unit 1 were described as intensely altered (de Ronde et al., 2019a). It appears that lithologic strength is the primary factor for vein networks being found in volcaniclastic units.

For Site U1528, vein density has a weakly positive correlation with lithology, alteration, and discrete vein total. This correlation suggests that lithologic units with higher degrees of alteration will contain more veins. This may be best explained multiple factors forming a positive feedback system. Decreased integrity could allow more fracturing to provide fluids a preferred pathway for movement; increased fluid movement could contribute to higher alteration intensity, which could even further weaken the lithologic integrity. It is notable that the correlation between vein density and discrete vein total is weakly positive, compared to the very moderately positive correlation of fracture density and discrete fracture total at Site U1528. This weakly positive correlation implies that a higher number of veins does not necessarily mean a higher number of discrete veins. With volcaniclastic rocks as the main host of veins, it is possible network veins increased vein density without creating more discrete veins. This could be due to low fluid pressure preventing discrete fractures from forming, or because the volcaniclastic rock is too weak to host a discrete fracture. Lithology has a very weak positive correlation with alteration as seen at Site U1527. There is also a very weakly positive correlation with lithology and discrete vein total at Site U1528. Although discrete veins are possible, volcaniclastic rocks

5.3 Thin Section Analysis

      Sites U1527 and U1530 were expected to share similar mineralogical vein fill,

given their proximity to each other on the caldera wall. Both sites do contain quartz as a

dominant mineral fill, but samples from both sites do not show the expected

accompanying minerals, such as chalcopyrite or bornite, found in high temperature, gas

poor, metal rich, moderately acidic (Type I) hydrothermal fluids (Humphris et al., 1995;

de Ronde et al., 2011). The presence of clay minerals observed in the veins can likely be

attributed to hydrothermal fluid alteration of the host rock during vein formation

(Haymon 1986). Site U1530 samples contain anhydrite, which is typical of a Type I

hydrothermal fluid. Massiot (2022) details that Site U1530 has three different

mineralogical assemblages in separate depth intervals that correspond to low-to-high

temperatures. Perhaps the discrepancy in vein fill can be attributed to shifts in fluid

composition, temperature, and/or pH that prevented accompanying Type I minerals from

forming alongside quartz and anhydrite. It is likely the fluids that formed veins seen in

thin section are a subset of Type I fluids that are observed today (Tontini et al., 2019).

The presence of anhydrite at Site U1530 may indicate the role of seawater down-welling.

Tontini et al. (2019) suggests this location as a site of shallow circulation, wherein colder

seawater moves down while warmer hydrothermal fluids are ejected via the venting field.

Site U1530 is seated within a chimney venting field, so it was expected to be primarily an

upwelling zone. However, vein fill and temperature logs (Massiot et al., in press)

indicate Site U1530 is a downwelling zone. The mixing of these two fluids of differing

temperatures may account for the precipitation of anhydrite to form venting structures

(Guo et al., 2020). The observation of anhydrite likely indicates the presence of heated

seawater and can explain why Sites U1527 and U1530 have different mineralogical assemblages despite both being seen at Type 1 fluids.

The majority of veins at Site U1528 contained anhydrite as their primary fill, which is not typical of low temperature, low pH, gas rich (Type II) hydrothermal fluids (Humphris et al., 1995, de Ronde et al., 2011). The presence of anhydrite reflects higher temperatures (Humphris et al., 1995). Anhydrite present in the resurgent cone may indicate an increase in temperature of fluids from interaction with the deeper magmatic region and/or fluids (de Ronde et al., 2011; Gruen et al., 2012). The fluids measured today do not seem to match fluids that formed these veins, based on mineralogical observations. It is likely that the fluids changed over time.

Of the 43 veins observed, 6 (14%) contain fibers that show growth patterns (Table 6.9). Four of those veins display antitaxial mineral fiber growth patterns with a suture line visible near center of the vein. Two veins show syntaxial mineral fiber growth pattern indicated by a less prominent suture line near the vein wall. Vein mineral fibers typically grow perpendicular to the vein wall in extensional veins, unless sheared or otherwise displaced (Bons et al., 2012). Vein fibers are also only expected to form under a consistent stress field such that the fibers grow towards the least compressive stress. If there is no preferential orientation of the least compressive stress, vein fibers may not form. Veins cause by regional tectonics would be expected to have vein fibers that plunge parallel to the extension direction. For veins generated from episodic caldera collapse or fluid overpressure, the dip of these veins is likely to be randomly distributed, and therefore fibers may not form or they would not follow any orientation pattern (Meng et al., 2019). Based on thin section observations, the overall lack of oriented fibers

suggests that regional extension does not play a large role in the formation of veins at Brothers volcano, which also matches the results from reorienting fractures and veins (see above). Instead, fluid overpressure and episodic caldera collapse may play a larger role in vein formation.

In Hole U1530, an older vein of quartz is cross-cut by a younger vein of quartz + anhydrite + gypsum. It appears as though a change in fluids happened at some point in time, allowing for the difference in vein fill. Also seen in Hole U1530 is a quartz vein that has been over grown by pyrite on one side. This could indicate a variability in fluid types: one fluid precipitated the quartz, while another fluid precipitated pyrite. This may relate to colder seawater interactions, which can lead to pyrite precipitation in veins connected to anhydrite venting structures (Guo et al., 2020). A change in fluids may be further supported by a "Y" shaped vein in Hole U1528. Although the primary fill is gypsum for both branches and the trunk, the absence of UCM2 in the older vein may indicate a subtle change in fluids. Crack-seal mechanisms, which can indicate reopening of veins and show generational deformation events, were not directly observed in thin section samples (i.e., no observable crack-seal fiber growth) (Ramsay, 1980). In several instances some of veins showed UCM1/2 on the outer edges of the vein, which may at first appear to be from reopening. However, it is likely that the clay minerals are due to alteration of the host rock. Perhaps if other minerals (quartz, pyrite, etc.) were seen with the clay, it may be from a reopening event. It is equally likely that hydrothermal fluid alteration of the rock wall accounts for the deposits of clay minerals on the edge of some veins. The relatively low abundance of oriented fibers suggests that vein generation

methods are largely episodic, and that fluid overpressure and caldera collapse plays a larger role in vein creation than regional tectonics.

5.4 Fluid Flow Summary

Based on the data and discussion presented here, fluid flow at Brothers volcano appears to be largely independent of regional extension. Regional extension may require more time to imprint upon more episodic controls for fracture/vein formation. It is likely that fluid overpressure or episodic collapse contribute the greatest to fracture generation, creating preferred pathways for hydrothermal fluids to ascend to the seafloor. Seawater may be incorporated into shallow circulation cells such as those suggested at Site U1530, or may move via primary/secondary porosity through the lithology to meet rising magmatic fluids. Differences in mineralogical observations indicate a likely variance in fluid composition over time, which can reflect the role of the seawater and/or the magma chamber/reservoir on the fluids.

CHAPTER VI – CONCLUSION

This caldera-wide study of fractures and veins reoriented to true geographic orientation was not able to determine if regional extension is a dominant method of planar feature generation. Sites on the caldera wall show increased presence of planar features in areas of specific alteration types, suggesting that fluid movement and subsequent alteration are of greater consequence. Downcore correlations of several key characteristics support this claim, and also indicate a more prominent presence of discrete veins in tougher rocks (lava flows) and network veins in volcaniclastic rocks. Thin section analysis between the three sites does not indicate regional tectonic extension as a driving force behind fracture and vein generation. Episodic events (fluid overpressure, caldera collapse) seem to play more of a role in the creation of fractures and veins at Brothers volcano.

Fractures and veins on the N and NW portion of the caldera wall (Sites U1527 and U1530, respectively) are likely generated during caldera collapse or from regional extension. The fractures dipping WNW and ESE, which are likely a conjugate set, may be from the regional extension; the SSE dipping cluster may be from caldera collapse. Fractures and veins found at Site U1528 on the resurgent cone are likely from episodic collapse, resurgent uplift, or fluid overpressure.

```python
#  Discrete Vein Total

    #Developers: Hunter Parisey, Robert Atnip

    input_file = input("Please Enter the path to the input file...\n")

    output_file= input("Enter the desired output filepath with name...\n")




    with open(input_file) as file_obj:



        bins = []

        veins = []



        data = file_obj.read()

        data = data.splitlines()




        for line in data:

            temp = line.split()

            bins.append([float(temp[0]), 0])

            try:

                veins.append([float(temp[1]), float(temp[2])])

            except:
```

```python
            continue

    for i_bin in bins:

        for vein in veins:

            if (i_bin[0] < vein[0] < i_bin[0] + 0.09) or (i_bin[0] <   vein[1] < i_bin[0]
+ 0.09) or (vein[0] < i_bin[0] and vein[1] > i_bin[0] + 0.09):

                i_bin[1] += 1

    outputFile = open(output_file, "w")

    for line in bins:

        outputFile.write(str(line[0]) + "," + str(line[1]) + "\n")

outputFile.close()
```

APPENDIX B – Thin Section Tables

Table 6.1

Hole U1527C Thin section observation

Thin Section Sample Number	Vein ID	Depth (mbsf)	Dominate Mineral Fill	Accompanying Minerals	Thickness (mm)	Visible Growth Orientation
1527C-13R-2-107-111 cm	V27C-1	202.10-202.20	Quartz	N/A	0.375-1	No
1527C-17R-2-53-58 cm	V27C-2	220.65-220.75	Quartz	UCM2, pyrite	0.05-0.15	Yes, antitaxial
1527C-17R-2-53-58 cm	V27C-3	220.65-220.75	Quartz	UCM2, pyrite	0.3-0.4;	Yes, antitaxial
1527C-17R-2-53-58 cm	V27C-4	220.65-220.75	Quartz	UCM2, pyrite	0.05-0.2	Yes, antitaxial

Table 6.1 Continued

1527C-17R-2-53-58 cm	V27C-5	220.65-220.75	Quartz	UCM2, pyrite	0.05-0.2	No

Table 6.2

Observed thin section veins at Hole U1527C: lithologies and alteration types

Vein ID	Lithology	Alteration Type	Fill
V27C-1	2b	IIa	Quartz
V27C-2	2b	IIa	Quartz
V27C-3	2b	IIa	Quartz
V27C-4	2b	IIa	Quartz
V27C-5	2b	IIa	Quartz

Table 6.3

Hole U1530A thin section observation

Thin Section Sample Number	Vein Assignment	Depth (mbsf)	Dominate Mineral Fill	Accompanying Minerals	Thickness (mm)	Visible Growth Orientation
1530A-12R-1-109-113 cm	V30A-1	60.50-60.60	Quartz, pyrite	N/A	0.05-0.25	Yes, syntaxial
1530A-12R-1-109-113 cm	V30A-2	60.50-60.60	Quartz, Anhydrite, Gypsum	N/A	0.375-1	No
1530A-12R-1-109-113 cm	V30A-3	60.50-60.60	Quartz, Anhydrite, Gypsum	N/A	0.375-1	No

Table 6.3 Continued

1530A-50R-1-48-50 cm	V30A-4	242.30 - 242.40	Quartz, UCM1	N/A	1.5-2.25	No
1530A-50R-1-48-50 cm	V30A-5	242.30 - 242.40	Quartz, UCM1	N/A	0.625-1.5	No
1530A-50R-1-48-50 cm	V30A-6	242.30 - 242.40	Quartz, UCM1	N/A	1-2	No
1530A-50R-1-48-50 cm	V30A-7	242.30 - 242.40	Quartz, UCM1	N/A	0.625-1.5	No

Table 6.3 Continued

1530A-50R-1-56-58 cm	V30A-8	242.40 - 242.50	Quartz, UCM1	N/A	0.1-0.15	No
1530A-50R-1-56-58 cm	V30A-9	242.40 - 242.50	UCM1	N/A	1.5-2	No
1530A-53R-1-13-15 cm	V30A-10	256.40 - 256.50	UCM1	Pyrite	1.5-4	No
1530A-55R-2-4-7 cm	V30A-11	267.33 - 267.43	Quartz, UCM1	N/A	0.25-1	No

Table 6.3 Continued

1530A-60R-1-54-56 cm	V30A-12	290.40 - 290.50	Quartz, pyrite	N/A	0.375-0.75	No
1530A-75R-1-68-71 cm	V30A-13	362.50 - 362.60	Anhydrite	Pyrite	1-8	No
1530A-88R-1-24-26 cm	V30A-14	424.50 - 424.60	Pyrite	Quartz, UCM1, UCM2	0.4-1.8	No

Table 6.4

Observed thin section veins at Hole U1527C: lithologies and alteration types

Vein ID	Lithology	Alteration Type	Fill
V30A-1	3	II	Quartz
V30A-2	3	II	Quartz, anhydrite
V30A-3	3	II	Quartz, anhydrite
V30A-4	5	V	Quartz
V30A-5	5	V	Quartz
V30A-6	5	V	Quartz
V30A-7	5	V	Quartz
V30A-8	5	V	Quartz
V30A-9	5	V	UCM1
V30A-10	5	V	UM1
V30A-11	5	V	Quartz
V30A-12	5	II	Quartz
V30A-13	5	IV	Anhydrite
V30A-14	5	IV	Pyrite

Table 6.5

Hole U1528A thin section observations

Thin Section Sample Number	Vein Assignment	Depth (mbsf)	Dominate Mineral Fill	Accompanying Minerals	Thickness (mm)	Visible Growth Orientation
1528A-8R-1-52-54 cm	V28A-1	50.30-50.40	Quartz	UCM1	0.625-1.85	No
1528A-9R-2-70-75 cm	V28A-2	56.80-56.90	Gypsum, Anhydrite	Quartz, UCM2	0.25-2	No
1528A-9R-3-2-4 cm	V28A-3	57.60-57.70	Gypsum	Pyrite, UCM1, UCM2	0.5-0.875	No
1528A-9R-3-2-4 cm	V28A-4	57.60-57.70	Quartz	Pyrite, UCM1	0.375-0.875	No

Table 6.5 Continued

1528A-9R-3-2-4 cm	V28A-5	57.60-57.70	Quartz	Pyrite, UCM1, UCM2	1.25-2.25	No

Table 6.6

Observed thin section veins at Hole 1528A: lithologies and alteration types

Vein ID	Lithology	Alteration Type	Fill
V28A-1	2a	III	Quartz
V28A-2	2a	II	Gypsum
V28A-3	2a	II	Gypsum
V28A-4	2a	II	Quartz
V28A-5	2a	II	Quartz

Table 6.7

Hole U1528D thin section observations

Thin Section Sample Number	Vein Assignment	Depth (mbsf)	Dominate Mineral Fill	Accompanying Minerals	Thickness (mm)	Visible Growth Orientation
1528D-9R-1-95-97 cm	V28D-1	96-96.10	Quartz	Pyrite, UCM1	0.75-0.875	No
1528D-9R-1-95-97 cm	V28D-2	96-96.10	Quartz, Anhydrite	N/A	0.08-0.125	No
1528D-9R-1-95-97 cm	V28D-3	96-96.10	Quartz, Anhydrite	N/A	0.08-0.125	No
1528D-14R-1-74-79 cm	V28D-4	120-120.10	Anhydrite	Quartz, Pyrite	0.25-0.875	No
1528D-14R-1-74-79 cm	V28D-5	120-120.10	Anhydrite	Quartz, Pyrite	0.05-0.25	No

Table 6.7 Continued

1528D-21R-2-61-66 cm	V28D-6	155-155.10	Anhydrite	Pyrite	0.05-0.15	No
1528D-34R-1-127-129 cm	V28D-7	216.50-216.60	Anhydrite	Pyrite	0.25-0.75	Yes, antitaxial
1528D-34R-1-127-129 cm	V28D-8	216.50-216.60	Anhydrite	Pyrite	0.125-0.75	No
1528D-39R-1-17-21 cm	V28D-9	239.40-239.50	Anhydrite	Pyrite	0.30-0.35	No
1528D-39R-1-17-21 cm	V28D-10	239.40-239.50	Anhydrite	Pyrite	0.30-0.40	No
1528D-39R-1-17-21 cm	V28D-11	239.40-239.50	Anhydrite	Pyrite	0.20-0.40	No
1528D-39R-1-17-21 cm	V28D-12	239.40-239.50	Anhydrite	Pyrite	0.0162-0.20	No

Table 6.7 Continued

1528D-43R-1-18-21 cm	V28D-13	258.60-258.70	Anhydrite	Pyrite, UCM1	0.175-0.3	No
1528D-43R-1-18-21 cm	V28D-14	258.60-258.70	Anhydrite	Pyrite, UCM1	0.10-0.20	No
1528D-51R-2-27-30 cm	V28D-15	298.60-298.70	Pyrite, gypsum	Anhydrite, UCM1	0.625-0.875	Yes, antitaxial
1528D-51R-2-27-30 cm	V28D-16	298.60-298.70	Gypsum, anhydrite	N/A	0.425-0.55	No
1528D-55R-1-39-42 cm	V28D-17	316.40-316.50	Anhydrite	UCM1, USDM	0.15-0.20	No
1528D-55R-1-39-42 cm	V28D-18	316.40-316.50	Gypsum, Anhydrite	Pyrite	0.04-0.06	No
1528D-55R-1-39-42 cm	V28D-19	316.40-316.50	Anhydrite	Pyrite	0.22-0.26	No

Table 6.8

Observed thin section veins at Hole U1528D: lithologies and alteration types

Vein ID	Lithology	Alteration Type	Fill
V28D-1	2a	III	Quartz
V28D-2	2a	III	Quartz, anhydrite
V28D-3	2a	III	Quartz, anhydrite
V28D-4	2a	II	Anhydrite
V28D-5	2a	II	Anhydrite
V28D-6	2b	III	Anhydrite
V28D-7	2c	II	Anhydrite
V28D-8	2c	II	Anhydrite
V28D-9	2c	III	Anhydrite
V28D-10	2c	III	Anhydrite
V28D-11	2c	III	Anhydrite
V28D-12	2c	III	Anhydrite
V28D-13	2c	III	Anhydrite
V28D-14	2c	III	Anhydrite
V28D-15	3	II	Gypsum
V28D-16	3	II	Gypsum
V28D-17	3	III	Anhydrite
V28D-18	3	III	Gypsum
V28D-19	3	III	Anhydrite

Table 6.9

Veins with mineral fiber orientation

Vein ID	Lithology	Alteration Type	Depth	Fiber Direction
V27C-2	2b	IIa and IIb	220.65-220.75	Up-core
V27C-3	2b	IIa and IIb	220.65-220.75	Up-core
V27C-4	2b	IIa and IIb	220.65-220.75	Up-core
V30A-1	3	II	60.50-60.60	Up-core
V28D-7	2c	IIc	216.50-216.60	Sub-vertical
V28D-15	3	III	298.60-298.70	Sub-vertical

REFERENCES

Acocella, V., Cifelli, F., and Funiciello, R., 2000, Analogue models of collapse calderas
and resurgent domes: Journal of Volcanology and Geothermal Research, v. 104, no.
1–4, p. 81–96.

Al-Harthi AA, Al-Amri RM, Shehata WM, 1999, The porosity and engineering
properties of vesicular basalt in Saudi Arabia. Engineering Geology, vol. 54, p.
313–320

Allmendinger, R. W., Cardozo, N., and Fisher, D., 2012, Structural geology algorithms:
Vectors and tensors in structural geology: Cambridge University Press.

Anderson, E. M., 1951, Dynamics of Faulting and Dyke Formation with Application to
Britain, 2nd ed. Edinburgh: Oliver & Boyd

Baker, E.T., Walker, S.L., Embley, R.W., and De ronde, C.E.J., 2012, High-Resolution
Hydrothermal Mapping of Brothers Caldera, Kermadec Arc: Economic Geology, v.
107, no. 8, p. 1583–1593.

Bons, P.D., Elburg, M.A., and Gomez-Rivas, E., 2012, A review of the formation of
tectonic veins and their microstructures: Journal of Structural Geology, v. 43, p. 33–
62.

Cardozo, N., and Allmendinger, R.W., 2013, Spherical projections with OSXStereonet:
Computers and Geosciences, v. 51, p. 193-205

Coumou, D., Driesner, T., and Heinrich, C.A., 2008, The Structure and Dynamics of
Mid-Ocean Ridge Hydrothermal Systems: no. September, p. 1825–1829.

Cucci, L., Di Luccio, F., Esposito, A., and Ventura, G., 2017, Vein networks in
hydrothermal systems provide constraints for the monitoring of active volcanoes:

Scientific Reports, v. 7, no. February, p. 1–8.

Embley, R.W., De Ronde, C.E.J., Merle, S.G., Davy, B., and Caratori Tontini, F., 2012, Detailed morphology and structure of an active submarine Arc caldera: Brothers volcano, Kermadec Arc: Economic Geology, v. 107, no. 8, p. 1557–1570.

Gamble, J.A., and Wright, I.C., 1995, Geological Structure and Magma Petrogenesis of an Active Backarc Rift Complex:

Gruen, G., Weis, P., Driesner, T., de Ronde, C.E.J., and Heinrich, C.A., 2012, Fluid-Flow Patterns at Brothers Volcano , Southern Kermadec Arc : Insights from Geologically Constrained Numerical Simulations: p. 1595–1611.

Guo, Z., Rüke, L. H., Fuchs, S., Iyer, K., Hannington, M. D., Chen, C., Tao, C., Hasenclever, J., 2020, Anhydrite-Assisted Hydrothermal Metal Transport to the Ocean Floor – Insights from Thermo-Hydro-Chemical Modeling, JGR Solid Earth, vol. 215, iss. 7

Hancock, P. L., A. Al-Kadhi, A. A. Barka, and T. G. Bevan, 1987, Aspect of analyzing brittle structures, Annales Tectonicae, 1, 5– 19

Haymon, R. M., Miriam, K., 1986, The formation of high temperature clay minerals from basalt alteration during hydrothermal discharge on the East Pacific Rise axis at 21° N: Geochimica et Cosmochimica Acta, v. 50, no. 9, p. 1933-1939

Heap, M. J., Wadsworth, F. B., Heng, Z., Xu, T., Griffiths, L., Velasco, A. A., Vairé, E., Vistour, M., Reuschlé, T., Troll, V. R., Deegan, F. M., Tang, C., 2021, The tensile strength of volcanic rocks: Experiments and models, Journal of Volcanology and Geothermal Research, vol. 418, 107348

Hubbert, M. K., Willis, D. G., 1957, Mechanics of Hydraulic Fracturing, AIME

Petroleum Transactions, vol. 210, p. 153-168

Humphris, S.E., Herzig, P.M., Miller, D.J., Alt, J.C., Becker, K., Brown, D., Brügmann, G., Chiba, H., Fouquet, Y., Gemmell, J.B., Guerin, G., Hannington, M.D., Holm, N.G., Honnorez, J.J., et al., 1995, The internal structure of an active sea-floor massive sulphide deposit: Nature, v. 377, no. 6551, p. 713–716.

Large, R.R., Allen, R.L., Blake, M.D., and Herrmann, W., 2001, Hydrothermal Alteration and Volatile Element Halos for the Rosebery K Lens Volcanic-Hosted Massive Sulfide Deposit , Western Tasmania: v. 96, no. 1981, p. 1055–1072.

Lipman, P. W., 1997, Subsidence of ash-flow calderas: relation to caldera size and magma-chamber geometry: Bulletin of Volcanology, v. 59, p. 198-218

Cécile Massiot, Iona McIntosh, Jeremy Deans, Sarah D. Milicich, Fabio Caratori Tontini, Cornel E. J. de Ronde, Ludmila Adam, Kannikha Kolandaivelu, Gilles Guerin, 2022, Petrophysical Facies and Inferences on Permeability at Brothers Volcano, Kermadec Arc, Using Downhole Images and Petrophysical Data. *Economic Geology*

Meng, Q., Hooker, J.N., and Cartwright, J., 2018, Quantifying vein attributes in massive mudstones (Triassic, SW England): Implications for progressive evolution of opening-mode fracture networks: Marine and Petroleum Geology, v. 98, no. June, p. 523–532.

Meng, Q., Hooker, J.N., and Cartwright, J., 2019, Progressive accretion of antitaxial crystal fibres: Implications for the kinematics and dynamics of vein dilation: Journal of Structural Geology, v. 126, no. February, p. 25–36.

Mordensky SP, Villeneuve MC, Kennedy BM, Heap MJ, Gravley DM, Farquharson JI,

Reuschlé T, 2018, Physical and mechanical property relationships of a shallow intrusion and volcanic host rock, Pinnacle Ridge, Mt. Ruapehu, New Zealand. J Volcanol Geotherm Res 359:1–20

Passchier, C.W., and Trouw, R.A.J., 2005, Microtectonics: Springer-Verlag Berlin Heidelberg.

Pollard, D. D, Aydin A., 1988, Progress in understanding jointing over the past century, GSA Bulletin, v. 100, no. 8, p. 1181-1204

Phillips, W.J., 1972, Hydraulic fracturing and mineralization: Journal of the Geological Society, v. 128, no. 4, p. 337–359.

Ramsay, J.G., 1980, The crack-seal mechanism of rock deformation: Nature, v. 284, no. 5752, p. 135–139.

Roberts, S., and Sanderson, D.J., 1998, FRACTAL ANALYSIS OF Sn-W MINERALIZATION FROM CENTRAL IBERIA: INSIGHTS INTO THE ROLE OF FRACTURE CONNECTIVITY IN THE FORMATION OF AN ORE DEPOSIT: Geology, v. 93, p. 360–365.

Robertson, E.A.M., Biggs, J., Cashman, K. V., Floyd, M.A., and Vye-Brown, C., 2016, Influence of regional tectonics and pre-existing structures on the formation of elliptical calderas in the Kenyan Rift: Geological Society Special Publication, v. 420, no. 1, p. 43–67.

Roche, O., Druitt, T.H., and Merle, O., 2000, Experimental study of caldera formation: v. 105, p. 395–416.

de Ronde, C.E.J., 2005, Evolution of a Submarine Magmatic-Hydrothermal System: Brothers Volcano, Southern Kermadec Arc, New Zealand: Economic Geology, v.

100, no. 6, p. 1097–1133.

de Ronde, C.E.J., Baker, E.T., Massoth, G.J., Lupton, J.E., Wright, I.C., Feely, R.A., and Greene, R.R., 2001, Intra-oceanic subduction-related hydrothermal venting, Kermadec volcanic arc, New Zealand: Earth and Planetary Science Letters, v. 193, no. 3–4, p. 359–369.

de Ronde, C.E.J., Humphris, S.E., Höfig, T.W., Brandl, P.A., Cai, L., Cai, Y., Caratori Tontini, F., Deans, J.R., Farough, A., Jamieson, J.W., Kolandaivelu, K.P., Kutovaya, A., Labonté, J.M., Martin, A.J., et al., 2019a, Expedition 376 summary: v. 376, no. July.

de Ronde, C.E.J., Humphris, S.E., Höfig, T.W., and Zhang, I., 2019b, and the Expedition 376 Scientists Proceedings of the International Ocean Discovery Program Volume 376 publications: v. 376.

de Ronde, C.E.J., Humphris, S.E., Höfig, T.W., Brandl, P.A., Cai, L., Cai, Y., Caratori Tontini, F., Deans, J.R., Farough, A., Jamieson, J.W., Kolandaivelu, K.P., Kutovaya, A., Labonté, J.M., Martin, A.J., et al., 2019c, Expedition 376 Methods: v. 376, no. July.

de Ronde, C.E.J., Humphris, S.E., Höfig, T.W., Brandl, P.A., Cai, L., Cai, Y., Caratori Tontini, F., Deans, J.R., Farough, A., Jamieson, J.W., Kolandaivelu, K.P., Kutovaya, A., Labonté, J.M., Martin, A.J., et al., 2019d, Expedition 376 Supplement: v. 376, no. July

de Ronde, C.E.J., Massoth, G.J., Butterfield, D.A., Christenson, B.W., Ishibashi, J., Ditchburn, R.G., Hannington, M.D., Brathwaite, R.L., Lupton, J.E., Kamenetsky, V.S., Graham, I.J., Zellmer, G.F., Dziak, R.P., Embley, R.W., et al., 2011,

Submarine hydrothermal activity and gold-rich mineralization at Brothers Volcano ,
Kermadec Arc , New Zealand: p. 541–584.

Secor, D. T., 1965, Role of Fluid Pressure in Jointing, American Journal of Science, v.
263 p. 633-646

Stix, J., Kennedy, B., Hannington, M., Gibson, H., Fiske, R., Mueller, W., and Franklin,
J., 2003, Caldera-forming processes and the origin of submarine volcanogenic
massive sulfide deposits: Geology, v. 31, no. 4, p. 375–378.

Tontini, F., Tivey, M.A., de Ronde, C.E.J., and Humphris, S.E., 2019, Heat Flow and
Near-Seafloor Magnetic Anomalies Highlight Hydrothermal Circulation at Brothers
Volcano Caldera, Southern Kermadec Arc, New Zealand: Geophysical Research
Letters, v. 46, no. 14, p. 8252–8260.

Unwin, H.E., Tuffen, H., Phillips, E., Wadsworth, F.B., and James, M.R., 2021, Pressure-
Driven Opening and Filling of a Volcanic Hydrofracture Recorded by Tuffisite at
Húsafell, Iceland: A Potential Seismic Source: Frontiers in Earth Science, v. 9, no.
June.

Walker, G.P.L., 1984, represent a volume deficit of about 45 km: v. 89, p. 8407–8416.

Wright, I.C., 1994, Nature and tectonic setting of the southern Kermadec submarine arc
volcanoes: An overview: Marine Geology, v. 118, no. 3–4, p. 217–236.

Wright, D.J., Bloomer, S.H., MacLeod, C.J., Taylor, B., and Goodlife, A.M., 2000,
Bathymetry of the Tonga Trench and Forearc: A map series: Marine Geophysical
Researches, v. 21, no. 5, p. 489–511.

Wright, I.C., and Gamble, J.A., 1999, Southern Kermadec submarine caldera arc
volcanoes (SW Pacific): Caldera formation by effusive and pyroclastic eruption: